

Chapter 11

THE STRUCTURE AND DEGRADATION OF INTACT PLANT CELL WALL
 MATRICES BY ^{13}C CPMAS NMR AND RELATED TECHNIQUES

Peter L. Irwin

TABLE OF CONTENTS

I.	Introduction	338
II.	Spectroscopic Problems Associated with Plant Cell Walls	338
	A. Dehydration	338
	B. Paramagnetic Ion Contamination	340
	C. Differential ^{13}C Signal Response Based Upon Proximity to Near Neighbor ^1H s	341
III.	The Primary Structure, Molecular Motion, and Degradation of Higher Plant Cell Wall Constituents	343
	A. A Comparative Study of the Molecular Motion of Cellulose, Ca PGA Gels, and Intact Cell Wall Complexes	343
	B. Polygalacturonan Structural Similarity between Tissues of Different Physiological Stage	345
	C. Changes in Cell Wall Polygalacturonan Conformation and Flexibility during the Time Coincident with Dissolution of the Middle Lamella	346
IV.	Conclusion	353
	References	354

I. INTRODUCTION

At the most general level of our understanding, the primary cell wall and middle lamellar complex of higher plant tissues¹ is considered to be a three phase system which is made up of a "crystalline" component (cellulose), a "matrix" component (the acid sugar-containing polymers or pectic polysaccharides and hemicellulose, etc.) as well as a "packing" component (bound H₂O). The architecture of the cell wall system, beyond simple primary structure, is not well understood,² albeit great advances have been made with regard to the three dimensional arrangement of cellulose microfibrils in certain plant tissues.

Over the last 5 years, work in the author's laboratory has centered on acid sugar-containing polysaccharides (e.g., polygalacturonans) as they exist, intact, in the cell wall complex.³⁻⁷ Specifically, we have been addressing the process of cell wall separation,⁸ which is believed to be due to the dissolution of the middle lamella (the electron dense region between adjacent cell walls) in certain agriculturally important commodities (e.g., *Malus pumila* fruit), because the physicochemical mechanism of and the ability to modulate this process are obscure. In many climacteric fruit crops (those which have a marked increase in ethylene synthesis and respiratory activity during fruit ripening), the degradation of the middle lamella or cell wall separation process is caused, at least in part, by the action of specific random-cleaving polygalacturonan hydrolases (endoPG). The apple system is unique because cell separation occurs without a detectable increase in endoPG activity^{9,10} even though there is a marked increase in cell wall polyuronide solubility.¹¹

In this chapter, ¹³C cross-polarization and magic angle spinning (CPMAS) NMR and other magnetic resonance experiments are presented which address questions regarding the higher order structure, molecular motion, and degradation of polygalacturonan blocks in intact cell wall polymers as a function of the cell separation process and specific enzymatic degradation. These molecular spectroscopic techniques are the major methods available for studying the dynamic and structural properties of individual components in heterogeneous solid materials.^{4,6,12} Such experiments are of interest because bulk mechanical properties of polymeric materials, such as a cell wall complex, can be related to polymer chain dynamics and molecular motions.¹²⁻¹⁴

II. SPECTROSCOPIC PROBLEMS ASSOCIATED WITH PLANT CELL WALLS

Before proceeding with a discussion of higher plant cell wall structure and degradation, there is justification to mention several factors which complicate the interpretation of relaxation time and ¹³C CPMAS NMR studies.

In the cross-polarization process, ¹⁵H magnetization is at equilibrium with the surroundings (lattice) and is proportional to the number of ¹Hs in the sample and is inversely proportional to the lattice "spin temperature". In order to observe the dilute ("hot") ¹³C species, these spins are induced to thermally interact with the abundant ("cold") ¹Hs by turning on a rf field of amplitude H_{1C} along the x axis of the ¹³C rotating frame. The magnitude of H_{1C} is arranged to fulfill the Hartman-Hahn condition ($\gamma_H H_{1H} = \gamma_C H_{1C}$) so that the two spin systems come to equilibrium with respect to spin temperature or magnetization. The rate at which ¹H-induced ¹³C magnetization increases is equal to T_{CH}⁻¹. At longer contact times, the ¹³C signal diminishes due to ¹H rotating frame spin-lattice relaxation (T_{1ρH}):

A. Dehydration

In Table I, ¹⁶CPMAS NMR ¹³C T_{1ρ} and T_{CH} data, calculated from the Na⁺-polygalacturonate (NaPGA; Sigma Chemical Co.) carbonyl (C=O) signal, are presented as a function of degree of dryness of the powders as well as the presence of other, non-acid sugar, constituents (e.g., cellulose). As shown previously,^{15,17,18} T_{CH}, the reciprocal ¹H-¹³C polarization transfer rate,

Table 1
EFFECT OF DEHYDRATION AND CELLULOSE ON C=O
RECIPROCAL ^1H - ^{13}C POLARIZATION TRANSFER RATE (T_{CH})
AND ^{13}C $T_{1\rho}$ ¹⁶

Drying technique/treatment	$T_{\text{CH}} \pm \text{SE}/\mu\text{s}$	$^{13}\text{C}=\text{O } T_{1\rho} \pm \text{SE}/\text{ms}$
Freeze-dried NaPGA + cellulose	298.0 \pm 22	18 \pm 1.00
Freeze-dried NaPGA ^a	214.0 \pm 13	23 \pm 1.00
NaPGA-lab ^b	143.0 \pm 10	7 \pm 0.32

Note: Peak intensities were used for the calculation of ^{13}C $T_{1\rho}$ and T_{CH} relaxation parameters by standard literature least square methods.¹¹ SEs were calculated from the least squares analysis of all data.

- ^a Dissolved in H_2O and freeze dried immediately before CPMAS NMR experiment.
- ^b Same as above without freeze drying (e.g., from the bottle).

depends upon a correlation time (τ_c) as well as ^{13}C - ^1H angular (with respect to the static magnetic field) and distance terms. $\text{C}=\text{O } T_{\text{CH}}$ differences between the two NaPGA samples is probably related to differences in the degree of polymer hydration since the treatment labeled "freeze dried-NaPGA" (Table 1) was lyophilized immediately prior to T_{CH} measurement. The "NaPGA-lab" treatment was stored at room temperature without prior lyophilization or other special drying treatment. Other evidence for differences in polymer hydration is that the $^{13}\text{C } T_{1\rho}$ data for these same samples were different by a factor of approximately three which argues for rather large differences in carboxylate group motion. These data indicate that improper drying techniques can cause significant differences in the rate of cross-polarization, via a increase in the average number of near neighbor ^1H s (T_{CH}), or an increase in the molecular motion ($^{13}\text{C } T_{1\rho}$) and, thus, could be problematic with regard to quantitative comparisons between cell wall treatments as well as comparisons of relaxation parameters. In this work, when performing solid state magnetic resonance experiments with *M. pumila* cell wall material,³⁻⁷ great care was taken to thoroughly dehydrate the samples via critical point drying procedures followed by storage *in vacuo* over dehydrated silica gel. This dehydration technique is preferred over freeze drying when working with intact native matrices since the specimens are not subjected to the surface tension forces, or the freezing and sublimation boundary conditions, associated with lyophilization which could alter the morphology of the sample.

Other evidence⁹ for H_2O -induced perturbations in the cross polarization process and ^1H spin-lattice relaxation are presented in Figure 1. In solids, the rate of ^1H spin-lattice relaxation ($\sim T_{1\text{H}}^{-1}$) is mediated by ^1H spin diffusion such that, in homogeneous samples with rapidly moving ^1H -rich domains (e.g., bound water or methyl groups), polymer $T_{1\text{H}}$ values will be inversely proportional to the molar concentration of these domains,¹⁹ assuming all other complicating factors are equivalent (i.e., molecular size). These data (Figure 1) indicate that polygalacturonan Ca^{2+} salts carry a certain degree of bound H_2O which is not easily removed by ordinary drying techniques since polyuronide $T_{1\text{H}}$ values declined as the carboxylate group binding sites filled with the divalent cation. If ionically associated bound H_2O were not present, one would expect either no change in $T_{1\text{H}}$ or an increase due to the cross-linking effect of Ca^{2+} on PGA motion. Other evidence for the presence of a significant degree of bound H_2O in "dehydrated" polymer salts is demonstrated (Figure 1, insert) by a decrease in both ring carbon (COH) and $\text{C}=\text{O } T_{\text{CH}}$. The $\text{C}=\text{O } T_{\text{CH}}$ values are about two times larger than those corresponding to ring carbons because PGA's acid functional group is unprotonated.^{17,18} As the available divalent cation binding sites filled the $\text{C}=\text{O } T_{\text{CH}}$ s diminished more (about 36%) than the COH values indicating that the bound water was associated with the cationic species. As these findings indicate, it is important that

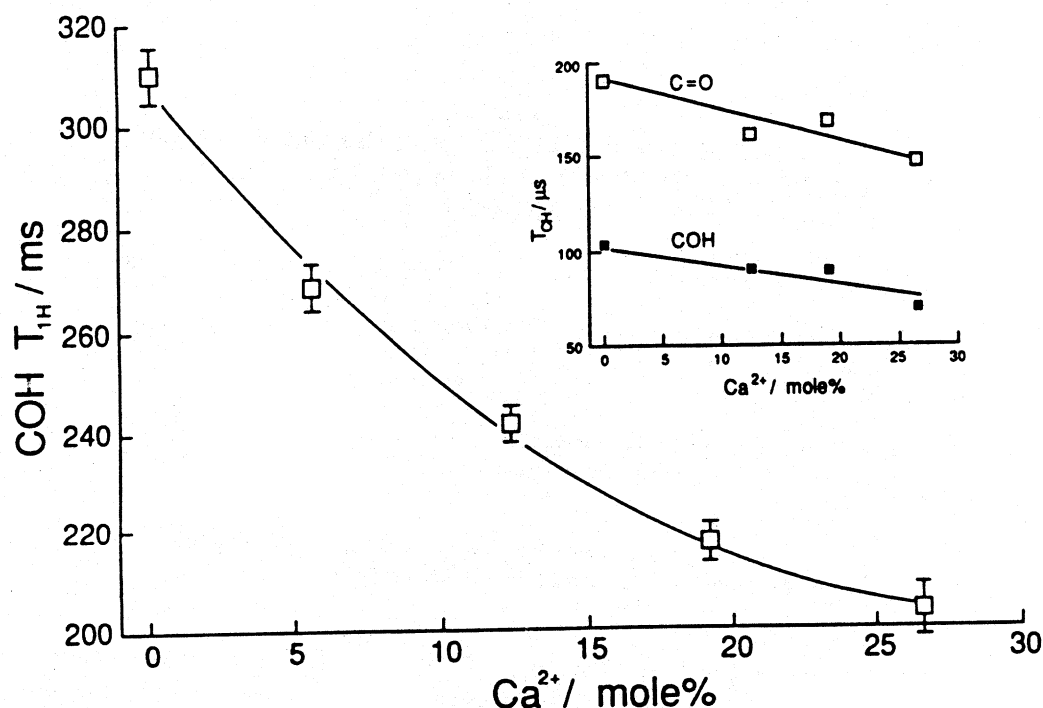


FIGURE 1. ^1H spin-lattice relaxation times (T_{1H}) and reciprocal ^1H to ^{13}C polarization transfer rates (T_{CH}) of dehydrated Ca^{2+} polygalacturonic acid salts. Vertical bars represent asymptotic SEs. About 500 mg polygalacturonic acid (H^+ form) was equilibrated in 25 ml of 800, 400, 100, 50, and 2 mM CaCl_2 in 75% (v/v) ethanol: H_2O to achieve 27 ± 2 , 19 ± 1 , 13 ± 4 , 5 ± 1 , and 0.15 ± 0.015 mol% bound Ca^{2+} , respectively. Samples were washed repeatedly with absolute ethanol, vacuum dried on scintered glass, and stored *in vacuo* at approximately 160 torr over silica gel for 2 to 3 weeks prior to CPMAS NMR experiments. Peak intensities were used for the calculation of ^1H T_1 and T_{CH} (the reciprocal ^1H - ^{13}C polarization transfer rate) relaxation parameters by standard literature least square methods.¹¹ SEs were calculated from the least squares analysis of all data. (From Irwin, P. L., Sevilla, M. D., and Stoudt, C. L., *Biochim. Biophys. Acta*, 842, 76, 1985.)

relaxation time studies of native polymer materials have equivalent levels of bound divalent cations. In the *M. pumila* cell wall experiments reported herein, the concentration of bound nonparamagnetic divalent cations were equivalent (about $1 \times 10^{-5} \pm 5 \times 10^{-6}$ mol \cdot g $^{-1}$).¹⁵

B. Paramagnetic Ion Contamination

Another problem related to solid matrices which contain anionic components is paramagnetic ion contamination which can induce extreme perturbations in various relaxation processes due to alterations in the local magnetic field (Figure 2, insert).⁵ In this experiment, Cu^{2+} -PGA was utilized as the paramagnetic species. Even at low concentrations of bound Cu^{2+} (e.g., 0.05 mol%), the ratio of C=O to anomeric C signal (contact time = 0.8 ms⁵) is about 0.9; this ratio is about 1.0¹⁶ without added Cu^{2+} . The difference between the contact time for maximal signal response ($S_{i,\text{max}}$ ^1H - ^{13}C contact time;¹⁶ Figure 2) of both anomeric and carbonyl carbons is equivalent (e.g., the slopes are equal), regardless of bound Cu^{2+} level, indicating that the differential signal response (Figure 2, insert) was due to a selective loss (about 10%) of the $^{13}\text{C}=\text{O}$ signal, possibly due to nonrandom Cu^{2+} binding as has been reported previously.^{4,6} It is possible to eliminate most paramagnetic species from acid sugar-containing wall materials via titration of the carboxylate group. Unfortunately, this procedure is also likely to remove a portion of the matrix polysaccharides.³ Bound Cu^{2+} is more problematic than species such as Mn^{2+} since it binds more tightly.^{5,6} Indeed, the titration of the Cu^{2+} -PGA powders with acidified EtOH could

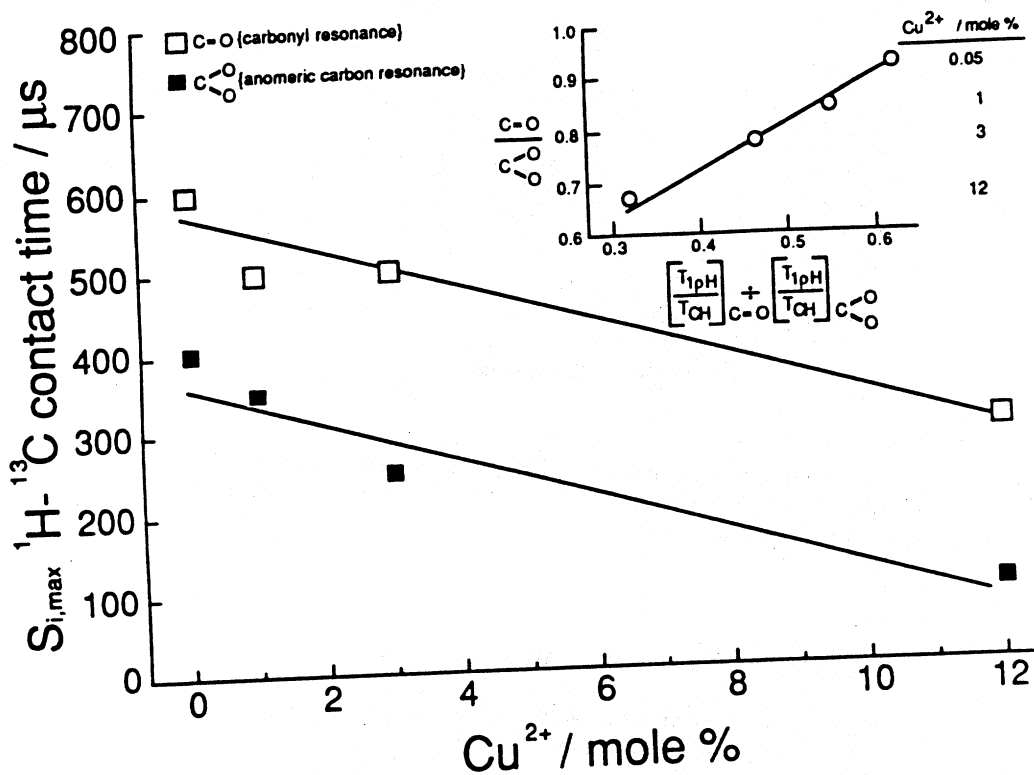


FIGURE 2. ^1H - ^{13}C thermal contact time for the observed maximum carbonyl and anomeric carbon signal ($S_{1,\text{max}}$ ^1H - ^{13}C contact time) as a function of mole percent bound Cu^{2+} on a polygalacturonic acid matrix.¹⁶ Inset figure: dependency of the ratio of carbonyl and anomeric carbon resonance integrals on the ratio of $T_{1\rho\text{H}}/T_{\text{CH}}$ for carbonyl and anomeric carbon resonances at different levels of bound Cu^{2+} . For these experiments, about 500 mg dry PGA powder was added to 25 ml of 100, 10, 1, and 0.1 mM CuCl_2 solutions in 95% (v/v) ethanol: H_2O and vortexed. After 7 h at room temperature, the samples were washed three times with an equal volume of absolute ethanol. The samples were dehydrated as described in Figure 1. (From Irwin, P. L., Gerasimowicz, W. V., Pfeffer, P. E., and Fishman, M., *Agric. Food Chem.*, 1985, 1197, 1985.)

not completely eliminate the paramagnetic effect.¹⁶ Cr contamination of laboratory glassware (from certain glass cleaning products) is a common source of undesired paramagnetic species.¹⁶ Because of these factors, it is advisable to select cell wall materials to be utilized for solid state NMR experiments, via atomic absorption spectrophotometry or EPR, which have no observable paramagnetic ion species. One should also make sure all laboratory glassware is paramagnetic ion free. The native apple cell wall materials discussed in this manuscript were examined by atomic absorption spectrophotometry as well as electron paramagnetic resonance spectroscopy (EPR) for the presence of paramagnetic species; none were detected.

C. Differential ^{13}C Signal Response Based Upon Proximity to Near Neighbor ^1H s

The last problem associated with CPMAS NMR of cell wall systems relates to quantitative comparisons of the ratio of carboxylate carbonyl resonances ($\text{C}=\text{O}$) or primary carbons ($-\text{CH}_3$) to total carbohydrate ring carbon resonances ($\text{COH} + \text{anomeric C}$). As shown before,⁵ such comparisons are likely to be quantitatively spurious if these samples have extremely different rates of ^1H to ^{13}C polarization transfer (T_{CH}^{-1}) and/or rotating frame spin-lattice relaxation ($T_{1\rho\text{H}}^{-1}$) as exemplified in Figure 3.¹⁶ In this graph, two calculated curves ($\text{COH } T_{\text{CH}} = 150 \mu\text{s}$, $\text{C}=\text{O } T_{\text{CH}} = 400 \mu\text{s}$; the $T_{1\rho\text{H}}$ for both is 4 ms) of relative signal vs. contact time are presented for directly protonated COH and remotely protonated $\text{C}=\text{O}$ groups. The contact time for maximal signal response for each functional group is extremely different. Also, the relative signal

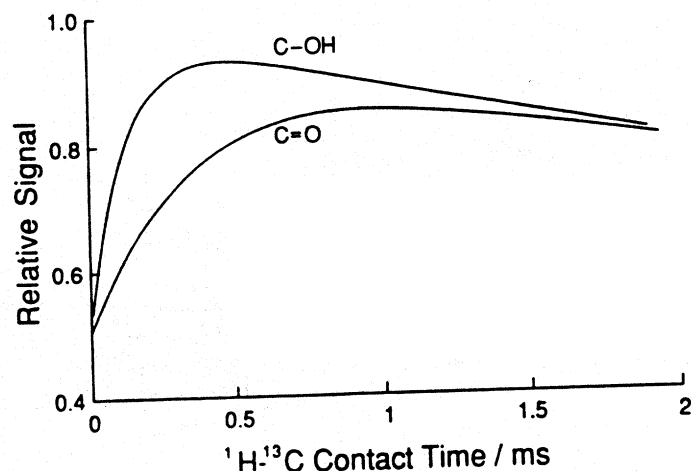


FIGURE 3. Calculated curves of ^1H to ^{13}C polarization transfer for nonspecific carbohydrate ring carbon (COH: $T_{\text{CH}} = 150 \mu\text{s}$; $T_{1\rho\text{H}} = 4 \text{ ms}$) and carbonyl (C=O: $T_{\text{CH}} = 400 \mu\text{s}$; $T_{1\rho\text{H}} = 4 \text{ ms}$) carbon resonances as a function of ^1H - ^{13}C contact time. In this relationship:

$$\int_0^{M_{1-\infty}} \frac{dM}{[M - M_{\text{max}}]} + \int_{M_{1=0}}^{M_{1-\infty}} \frac{dM}{M} = \int_0^t -\frac{dt}{T_{\text{CH}}} + \int_0^t -\frac{dt}{T_{1\rho\text{H}}}$$

M_{max} is the maximum magnetization observable assuming the $T_{1\rho\text{H}}$ process is negligible; t is the ^1H - ^{13}C thermal contact period.

amplitudes do not approach equivalence until relatively long contact times whereupon a 15 to 20% reduction in total potential signal was observed due to $T_{1\rho\text{H}}$ -mediated relaxation. Another example of this effect²⁰ is shown (Figures 4 and 5) for CPMAS studies on *Nitella translucens*^{21,22} cell walls. This algal species is interesting because the cell walls are quite large (up to several centimeters; can be treated as crystalline materials) and are made up almost entirely of primary wall constituents without the interconnecting middle lamella (the nodes were excised to facilitate the removal of the cytoplasmic components) between adjacent cell walls. In this example, one immediately notes the relatively large 19 ppm δ_{CH_3} resonance (Figure 4) which is typical for the primary C-6 of rhamnose or the methyl resonance of acetylated sugars; this constituent is ordinarily unobservable due to low concentrations in other primary cell wall/middle lamellar matrices, such as the apple system. The relative mole percentage of rhamnose or acetylated sugars in these algal cell walls is valuable to know since rhamnose is an important constituent of pectic polysaccharides and because this particular sugar was unreported in previous primary structural studies.^{21,22} Unfortunately, because of methyl group rotation,¹⁹ the cross-polarization process for the 19 ppm δ_{CH_3} is extremely different than the $\delta_{\text{C=O}}$ functionality or any other carbohydrate resonance (Figure 5) and, therefore, complicates the estimation of the relative molar composition of this sugar. In Figure 5, it is clear that the signal intensity, all of which were normalized such that the maximum signal was unity, for this CH_3 group diminished approximately 40% as the C=O magnetization approached its maximum at about 0.8 ms of ^1H - ^{13}C thermal contact. Even if these functional groups had equivalent T_{CH} and $T_{1\rho\text{H}}$ values quantitation would, at best, be difficult since the 19-ppm resonance is part of the shoulder of the major ring carbon resonances.

In the experiments reported herein, the contact time (0.8 ms) utilized for apple cell wall/middle lamellar matrices, which were compared quantitatively, produced precise, but not necessarily accurate, quantitative information³ even though C=O T_{CH} 's between compared

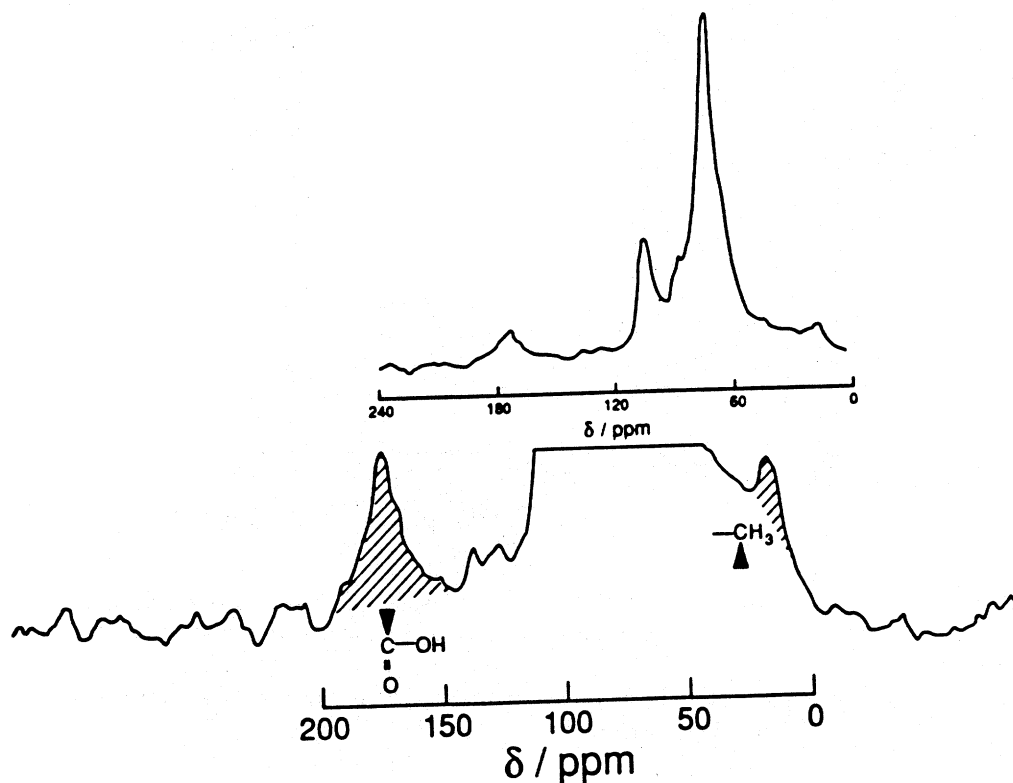


FIGURE 4. ^{13}C CPMAS NMR spectra of dehydrated *Nitella translucens* primary cell walls.²⁰ The 8-kHz wide NMR spectra were obtained at a ^{13}C frequency of 15 MHz; the ^1H decoupling field strength was 11 G. A total of 1024 (1k) data points were sampled and 0 filled to 4096 (4k) for data acquisition. All chemical shifts (δ) were assigned relative to the methyl resonance ($\delta = 17.36$ ppm) of hexamethylbenzene. Samples were spun approximately 2.4 kHz at the "magic angle" in a Kel-F bullet type rotor. This spectrum represents 20,000 transients collected with a ^1H - ^{13}C thermal contact period (contact time) of 0.8 ms. Samples were prepared by removing nodal lamellae and carefully squeezing out the cytoplasmic constituents in the presence of a 1% [w/v] solution of sodium dodecyl sulfate. Samples were dehydrated and critical point dried as described in Figure 8's caption.

treatments were different by a factor of about 50% (day 21 $\text{C}=\text{O}$ $T_{\text{CH}} = 381 \pm 38 \mu\text{s}$, day 0 $\text{C}=\text{O}$ $T_{\text{CH}} = 251 \pm 14 \mu\text{s}$; Figure 8).

III. THE PRIMARY STRUCTURE, MOLECULAR MOTION, AND DEGRADATION OF HIGHER PLANT CELL WALL CONSTITUENTS

A. A Comparative Study of the Molecular Motion of Cellulose, Ca PGA Gels, and Intact Cell Wall Complexes²³

As mentioned previously, the major structural carbohydrate constituents of the primary cell wall and middle lamellar complex of higher plants are cellulose (β 1 \rightarrow 4 glucans), hemicellulose (β 1 \rightarrow 3 and 4 glucans, xyloglucans, xylans) and pectin (α 1 \rightarrow 4 galacturonans with rhamnose, galactose, and other neutral sugars). McKay and co-workers²³ have utilized broadband (e.g., samples in a hydrated, but solid, state) ^1H magnetic resonance spectroscopic techniques to study the molecular motion of perdeuterated cellulose, Na and Ca PGA gels and isolated *Phaseolus vulgaris* hypocotyl cell walls (Figures 6 and 7) which have been fully "hydrated" in $^2\text{H}_2\text{O}$. Figure 6 shows typical ^1H time (spectra B and C, for cell wall and 8% Ca PGA gels, respectively) and frequency domain (spectrum A, Fourier transform of time domain spectrum C) spectra for the PGA gels and cell walls. Second moments ($\langle v^2 \rangle$, Equation 1) were calculated from all spectra; the $\langle v^2 \rangle$ is useful because, in solids, it is a function of the dipolar interactions between near

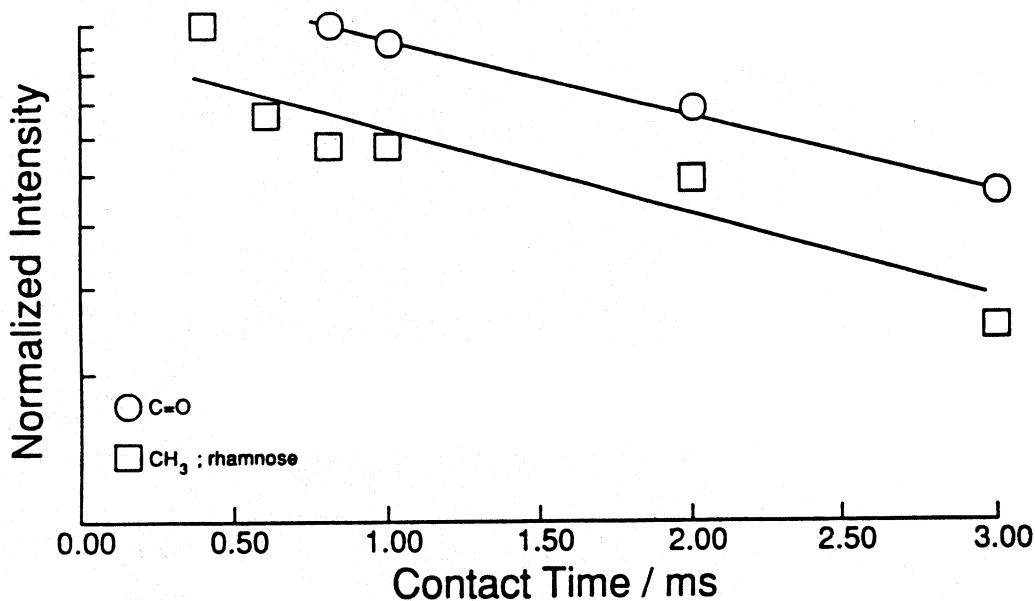


FIGURE 5. Contact time study of the carbonyl resonance (open circles) and the methyl group resonance (open squares) of dehydrated *Nitella translucens* cell walls.²⁰ Experimental conditions were as noted in Figure 4.

neighbor spins and is easily related to the spatial architecture of the ¹Hs in the various samples (Equation 2) as shown below:

$$\langle v^2 \rangle = \int_0^\infty \frac{(\omega - \omega_0)^2 f(\omega)}{2\pi} d\omega \quad (1)$$

and

$$\langle v^2 \rangle = \frac{9 \gamma^4 h^2}{20 N} \sum_j \sum_{k \neq j} \frac{1}{r_{jk}^3}$$

In these relations, $f(\omega)$ is the ¹H NMR lineshape, ω_0 is the angular Larmor frequency of the nuclei ($\omega = \pi\nu$), N is equivalent to the number of ¹Hs in the sample, r is the average distance between neighboring ¹Hs; γ , as well as h , have their usual values. The early part of the time domain spectrum (the free induction decay or FID) represents the motionally rigid components while the later part of the total FID results from the more mobile components. For cellulose, the early part of the FID decayed approximately 40% faster (a larger $\langle v^2 \rangle$) than the equivalent part of the intact cell wall system, which, in turn, was approximately 20% faster than the early part of the Ca²⁺ PGA gel's FID (Figure 6, subspectra B and C). This finding indicates that the time domain spectrum of the cell wall is roughly equal to the summation of the gel/cellulose FIDs. This finding makes sense since these individual constituents are about equal to each other in the primary wall complex of higher plants. Figure 7 shows a plot of the ratio of the cell wall $\langle v^2 \rangle$ ($\langle v^2 \rangle^T = \text{total } \langle v^2 \rangle$; $\langle v^2 \rangle^R = \text{rigid, or broadline, component } \langle v^2 \rangle$) as a function of sample temperature. Clearly, as the hydrating species begins to melt at about -5 to -10°C, the mobile component undergoes a greater motional averaging of the dipolar interactions than the rigid component

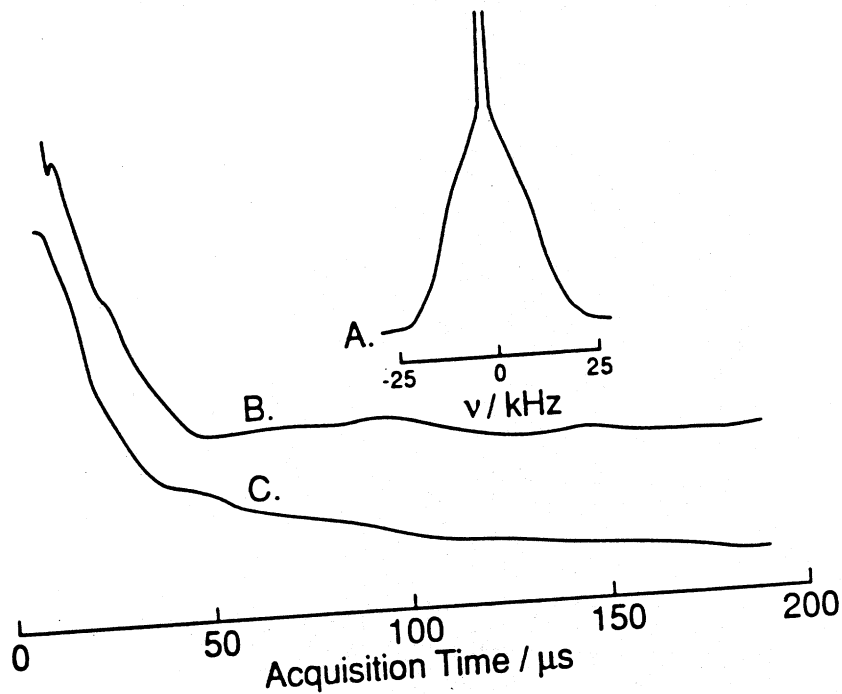


FIGURE 6. Frequency (A) and time domain (B and C) spectra of *Phaseolus vulgaris* (B) cell walls and CaPGA gels (A and C). $^1\text{H-NMR}$ results were acquired at 90 MHz. Na⁺ Polygalacturonic acid (PGA) was obtained from Sigma Chemical Co. A 2.5% [w/v] solution of PGA was made with $^2\text{H}_2\text{O}$ whereupon it was lyophilized and redissolved in $^2\text{H}_2\text{O}$ to make an 8% [w/v] solution. This solution was induced to gel by dialysis against a 10 mM CaCl_2 (in $^2\text{H}_2\text{O}$) solution for 18 h. *Phaseolus vulgaris* cell wall matrices were isolated from dark-grown 8-d-old hypocotyls. Hypocotyl sections, which had been stored at -20°C , were pulverized in a dry ice:ethanol bath, thawed, and ultrasonicated to remove bound cytoplasmic fragments. The resultant slurry was allowed to settle until two layers appeared; the upper layer (cell walls) were decanted and centrifuged at 200 $\times g$ for 15 min. The pelleted wall fragments were suspended in $^1\text{H}_2\text{O}$ and centrifuged twice to remove any residual cytoplasmic contamination whereupon the cell wall matrices were allowed to exchange with several changes of $^2\text{H}_2\text{O}$. Excess $^2\text{H}_2\text{O}$ was removed by vacuum filtration and the sample was weighed and packed into a 10-mm NMR tube. The samples prepared in this fashion contained about 4.7 g $^2\text{H}_2\text{O}$ per gram cell wall.²¹ For this figure, individual spectra were digitized from the original article²¹ and recreated on a 32 bit microcomputer. (From MacKay, A. L., Bloom, M., Tepfer, M., and Taylor, I. E. P., *Biopolymers*, 21, 1521, 1982. With permission.)

since $\langle v^2 \rangle^R$ diminishes only 16% while $\langle v^2 \rangle^T$ drops more than 60 to 70% and argues that the mobile cell wall components resulted from the most hydrated portions of the wall matrix. Unfortunately, $^2\text{H}_2\text{O}$, which was used in these studies as the hydrating species, has completely different hydration properties, at least with homopolygalacturonans,²⁰ than does $^1\text{H}_2\text{O}$. In this laboratory, it has been noted with spin-labeled PGA that $^2\text{H}_2\text{O}$ is a worse solvent than $^1\text{H}_2\text{O}$. In fact, EPR spin echo modulation studies on such samples hydrated in $^2\text{H}_2\text{O}$ show fewer bound $^2\text{H}_2\text{O}$ molecules than one would expect. Similar results²⁰ have been noted in $^2\text{H}_2\text{O}$ NMR spin echo studies of hydrated PGA.

B. Polygalacturonan Structural Similarity between Tissues of Different Physiological Stage

The major functionalities observed in ^{13}C CPMAS NMR spectra (Figure 8)⁵ of apple fruit cell wall material are the anomeric ($\delta = 105$ ppm) and nonspecific carbohydrate ring carbon ($\delta = 74$ ppm) resonances. These signals are not specific to any particular cell wall or middle lamellar component but result from the combined resonances of all carbohydrate ring carbons. However,

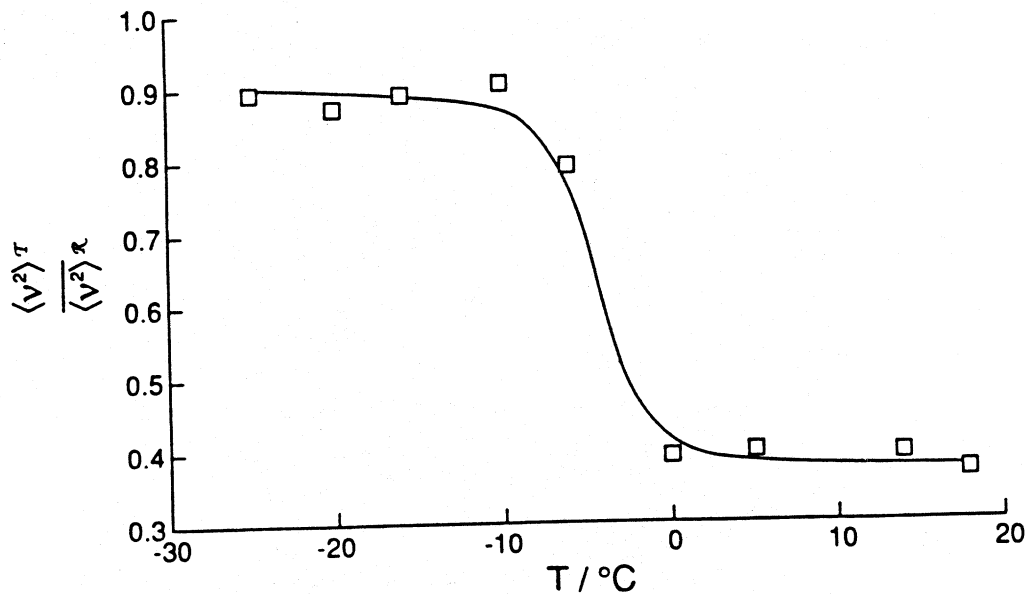


FIGURE 7. Dependency of $\langle v^2 \rangle^T / \langle v^2 \rangle^R$ on temperature in $^2\text{H}_2\text{O}$ -hydrated *Phaseolus vulgaris* cell walls. $\langle v^2 \rangle^T$ and $\langle v^2 \rangle^R$ represent the total components and the broadline component of the ^1H frequency domain spectral second moments, respectively. The authors²¹ estimated that the accuracy of the $\langle v^2 \rangle$ measurements were $\pm 5\%$. For this figure, individual data points from the original were digitized, $\langle v^2 \rangle^T$ divided by $\langle v^2 \rangle^R$ and plotted on a 32-bit microcomputer.

the carbonyl resonance ($\delta = 172$ ppm) results from cell wall components that contain carboxylate groups, most of which are due to the acid sugar-containing polymers.²⁴ Spectra (Figure 8) for the day 0 and 21 apple cell wall complex show that the ratio of the C=O to anomeric carbon resonance areas was about 0.3.⁵ Assuming a 5% (w/w) cell wall protein contribution to the C=O signal,²⁴ the day 0 and 21 treatments would have a total uronide content of approximately 24 and 25%, respectively. The degree of methyl esterification ($\delta = 54$ ppm) was also found to be similar between the two treatments (about $54 \pm 5\%$). Assuming proper conditions for quantitation exist ($T_{\text{CH}} \ll \text{contact time} \ll T_{1\rho\text{H}}$ [i.e., $T_{1\rho\text{H}}/T_{\text{CH}} \gg 1$]), these findings argue that the primary structure, or basic composition, of cell wall polyuronides does not change significantly during the course of the cell separation process.

Also arguing for structural similarity is the fact that the sequential⁴ divalent cation binding behavior of these samples were virtually identical (Figure 9).^{6,25} In Figure 9, day 0 and 21 (C=O $T_{1\rho\text{H}} = 333 \pm 12$ and 123 ± 15 ms, respectively) cell wall-bound Mn^{2+} line widths (ΔH_{pp}) are plotted as a function of cell wall bound Mn^{2+} concentration. ΔH_{pp} s were determined by comparing an empirical line broadening factor to computer-generated first derivative spectra.⁴ As the paramagnetic ion lattice filled, the ΔH_{pp} s, which have been shown to be a measure of Mn^{2+} near neighbor distances,^{4,6} were equivalent at either physiological stage. These data indicate that the lattice constants (κ) and, therefore, the lattice site molecular sizes²⁵ were similar. A comparable result was found with the Cu^{2+} salts.^{6,25}

C. Changes in Cell Wall Polygalacturonan Conformation and Flexibility during the Time Coincident with Dissolution of the Middle Lamella

Cell wall to wall separation in climacteric fruits, such as apple, has long been assumed to result from the direct action of various hydrolytic enzymes.^{26,27} However, in apple, the wall separation process⁸ is unusual since no random-cleaving polygalacturonase^{9,10} (endoPG) has been found while, concurrently, solubilization of polygalacturonans, the major constituent of

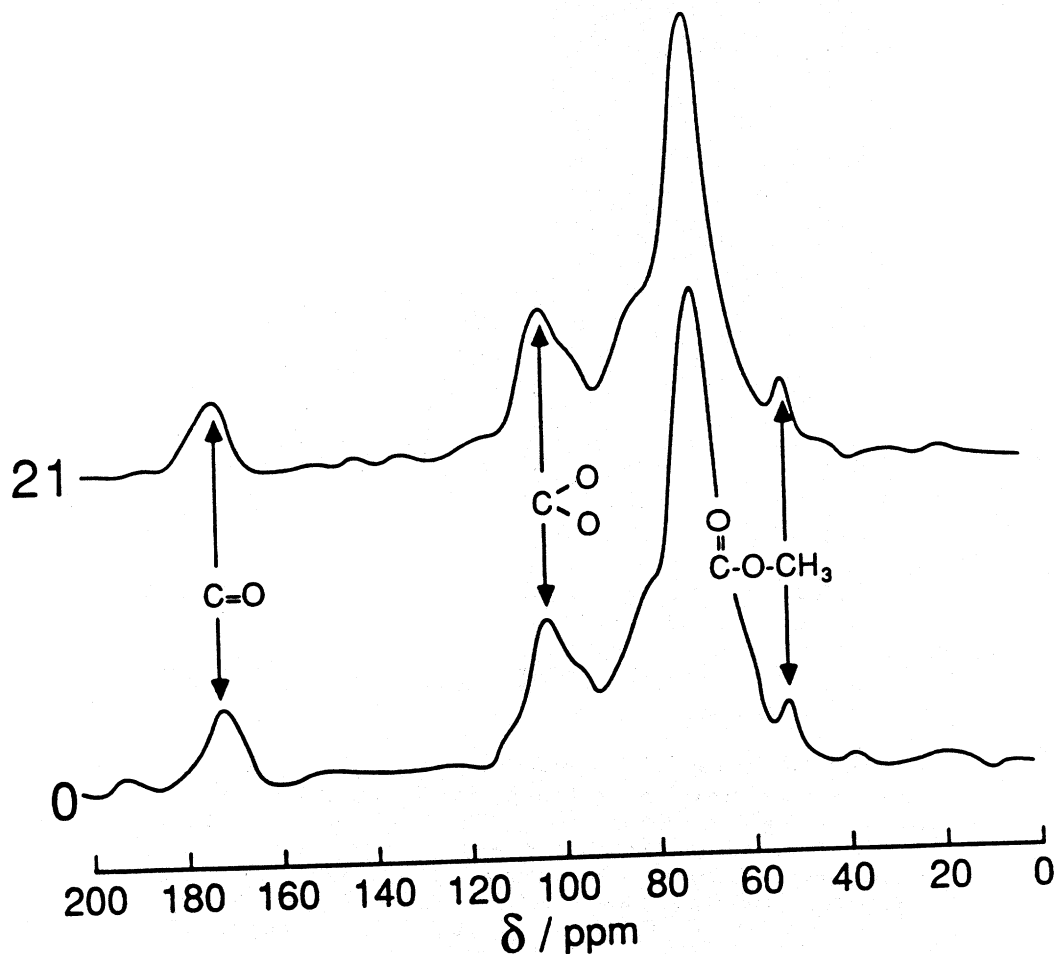


FIGURE 8. ^{13}C -CPMAS NMR spectra of dehydrated *Malus pumila* fruit cortical tissue ripened 0 and 21 d. Spectral conditions were as described in Figure 4. Peak areas were determined by triangulating to the baseline and taking three planimeter measurements per resonance. Spectra used for quantitative measurements were acquired by utilizing a 0.8-ms ^1H - ^{13}C thermal contact time. Apple fruit (cv. Golden Delicious) were obtained with the cooperation of the Beltsville Agricultural Research Center. Fruit were picked, randomized, and immediately stored at approximately 0°C in 1% (v/v) O_2 . After 1 month storage, fruit were removed and ripened for periods of 0, 4, 11, and 21 d at 20°C . Cortical tissues were cut into approximately $5 \times 5 \times 3$ mm sections and dipped in chilled 0.01 M CaCl_2 to inhibit oxidation. Cortical tissues were vacuum infiltrated consecutively 2 h or more in each of the following solutions: 20, 40, 60, and 80% ethanol: H_2O . The ethanol fixed cell wall complex was then equilibrated in 95% ethanol for 1 d with repeated solution replacement. Samples were further reduced in size to 1-mm sections and equilibrated 1 h each in three changes of absolute ethanol (100 ml/500 mg dry weight equivalent) followed by critical point drying. (From Irwin, P. L., Gerasimowicz, W. V., Pfeffer, P. E., and Fishman, M., *J. Agric. Food Chem.*, 1985, 1197, 1985.)

pectic substances, does increase.¹¹ Because matrix and primary cell wall polygalacturonans are somehow involved in the changes of plant tissue structure, it is of biochemical interest to study the localized molecular motions of uronide-containing polymers in intact cell walls during the cell separation process by utilizing noninvasive techniques, such as ^{13}C CPMAS NMR and solid state EPR spectroscopy.

Assuming the number of directly bonded and H_2O of hydration ^1H s remain constant, nonspecific carbohydrate ring carbon ^1H relaxation times ($\text{COH } T_{1\rho}$) are measures of polymer reorientation rates or motions averaged across all cell wall components. However, relaxation times measured from the $\text{C}=\text{O}$ resonance are inversely proportional to the motion of either carboxylate groups specifically, as measured by $^{13}\text{C}=\text{O } T_{1\rho}$, or to the motion or conformational flexibility of entire uronide-containing polymers, as measured by $^1\text{H } T_{1\rho}$ and $^1\text{H } T_1$.

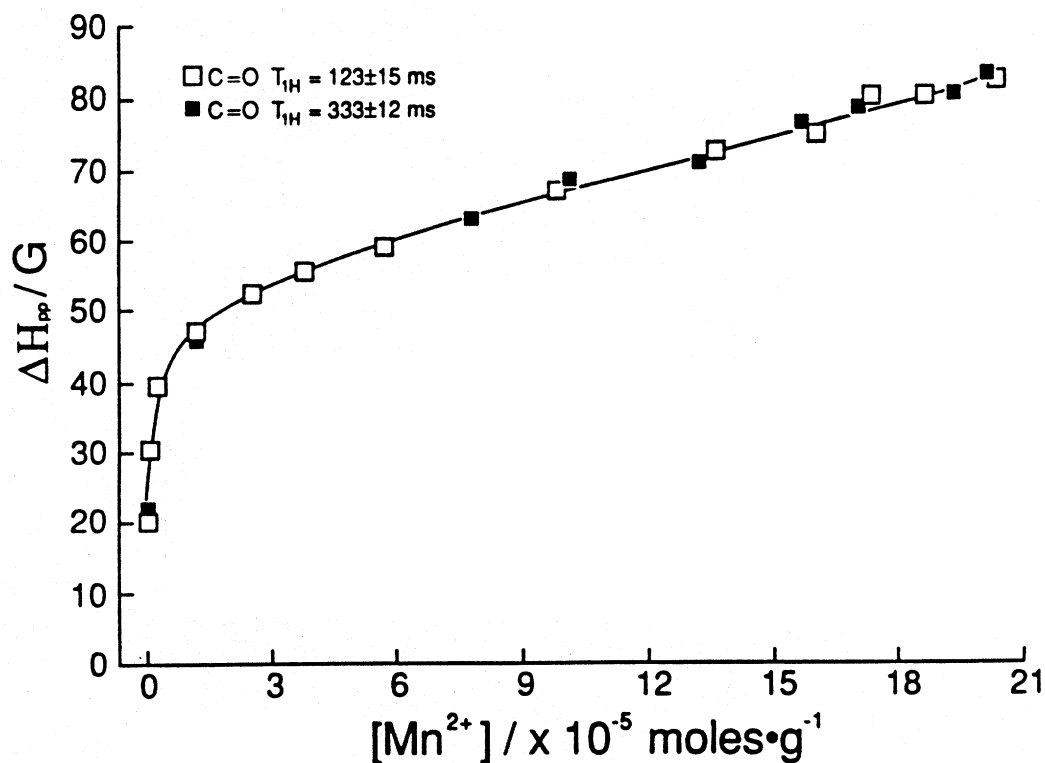


FIGURE 9. Cell wall bound Mn^{2+} concentration dependency of Mn^{2+} line width (ΔH_{pp}).²⁵ Open squares represent measurements taken from cell wall samples having a $C=O T_{1H}$ of 123 ± 15 ms. Closed squares represent measurements taken from cell wall samples having a $C=O T_{1H}$ of 333 ± 12 ms. Intact cortical tissues of apple fruit were prepared as detailed in Figure 8 and equilibrated at room temperature in 10 ml of various $MnCl_2$ concentrations in order to achieve a wide range of bound paramagnetic ions; critical point drying followed thereafter. All EPR spectra were obtained on a Varian Series E-109B spectrometer⁷ at various temperatures. Mn^{2+} spectral parameters were 1.6-mW microwave power; 4 to 32 min scan time; 1.6 to 2.0 kG scan range; 3224 G center field setting (H_0); about 9.1-GHz microwave frequency; 4-G modulation amplitude; and 100-kHz modulation frequency.

Rotating frame spin-lattice relaxation times of the $C=O$ resonance (Figure 10),³ which are measures of motions in the 10 to 100-kHz range,¹³ were measured from intact, ethanol-dehydrated and critical point dried tissues obtained from apple fruit before and after 21 days of ripening at 20°C. $^{13}C=O T_{1\rho}$ values decreased approximately 15% over this time period; the day 21 treatment $T_{1\rho C}$ was approximately 13% smaller than the NaPGA $T_{1\rho C}$ upon lyophilization within a cellulose matrix (33% [w/w]; Table 1).¹⁶ These data argue that some alteration has occurred in the size or higher order structure of pectic substances within the intact cell wall matrix. Confirmation of differences in cell wall carboxylate group motion were also obtained by way of $^{23}Na^+$ T_1 measurements (Figure 10, insert) of the polygalacturonan Na^+ salts in intact cell wall matrices. Cell wall-bound Na^+ T_2 s were estimated to be on the order of 0.22 ms ($T_1/T_2 \gg 1$) from the line width of the $^{23}Na^+$ resonance. From this knowledge one can argue that the change in $^{23}Na^+$ T_1 s with time was indicative of decreasing Na^+ binding site τ_c or increasing carboxylate group mobility. Therefore, the alteration of $^{23}Na^+$ T_1 s tends to agree with the $T_{1\rho C}$ results.

Evidence for increasing cell wall complex polygalacturonan main chain mobility, as a

Reference to brand or firm name does not constitute endorsement by the U.S. Department of Agriculture over others of a similar nature not mentioned.

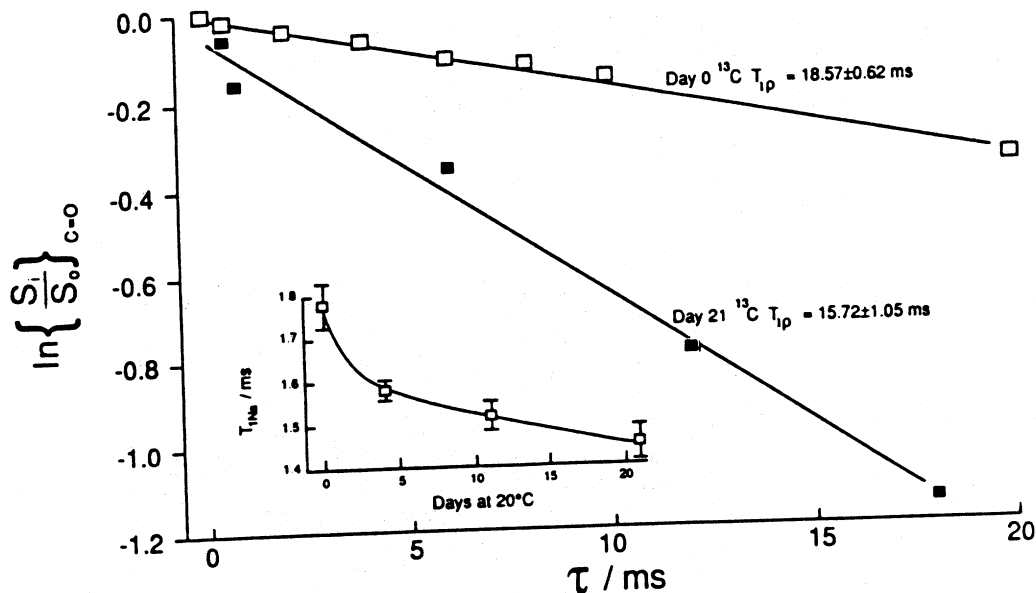


FIGURE 10. Natural log of normalized carbonyl signal intensities as a function of ^{13}C spin-locking time (τ) for cell wall samples ripened 0 and 21 d. Inset figure: plot of ^{23}Na T_{1p} s as a function of ripening time at 20°C . The calculated relaxation times are reported \pm S.E. Approximately 2 g of the fixed cell wall material from each treatment was washed three times in 180 ml H_2O and equilibrated 1 d in 1 M NaCl (pH 7) at 20°C . The samples were washed to remove unassociated Na^+ , equilibrated in absolute ethanol and critical point dried. Three or more 30-mg dry cell wall samples were washed three times in 10 ml pH 2 H_2O in order to remove bound Na^+ . Na^+ was analyzed by atomic absorption spectrophotometry using standard methods. ^{23}Na Spectra (± 25 -kHz sweep width) were obtained at 500 MHz (^1H frequency) by the University of Illinois School of Chemical Sciences NSF regional NMR facility (Dr. Eric Oldfield and Mr. Benjamin Montez). Samples were spun 3.7 kHz at the "magic angle". Peak intensities (100-Hz line broadening) were used for the calculation of T_{1p} s. The pulse sequence for the Na^+ experiments consisted of a train of ten 90° pulses separated with delay time of 10 μs followed by a variable delay (0.05 to 50 ms) during which T_1 relaxation occurred. Calculations were performed utilizing standard least squares analysis.¹⁵ (From Irwin, P. L., Pfeffer, P. E., Gerasimowicz, W. V., Pressey, R., and Sams, C. E., *Phytochemistry*, 23, 2239, 1984.)

function of the cell separation process or specific enzymatic (PG II from tomato) degradation, are presented in Figures 11 and 12, respectively. In these experiments, spin-lattice relaxation times measured from the carbonyl resonance ($\text{C}=\text{O}$ T_{1H}) were proportional to cell separation force (Figure 11)³ or PG II-induced soluble polyuronide production (Figure 12).³ Nonspecific carbohydrate ring carbon ^1H T_{1p} s ($\delta_{\text{COH}} = 74$ ppm; Table 2) displayed no such clear trend. The COH T_{1H} (Table 2) data might reflect an initial perturbation in total cell wall complex polysaccharide motion due to changes in the structure or architecture of the pectic polysaccharides, which make up nearly [1/3] of the total cell wall complex, followed by a gradual relaxation back to their initial state of mobility. The specific degradation of apple cell wall polygalacturonans by means of an endoPG induces a 42% (from about 160 ms to about 91 ms)³ drop in nonspecific ring carbon T_{1H} s which tends to support the concept that a change in the organization or size of cell wall-bound polygalacturonans induces motional perturbations in the entire complex. Unfortunately, due to the diversity of polymers represented by the total ring carbon signal, one cannot attribute these observed T_{1H} alterations to any one component. Cell wall ^1H T_{1p} values (Table 2) remained relatively constant during this time course study, indicating that lower frequency modes of reorientation²⁸ have not been altered.

Cell wall separation-associated perturbations in polygalacturonan main chain flexibility have also been confirmed utilizing paramagnetic ion spin-spin coupling differences as a

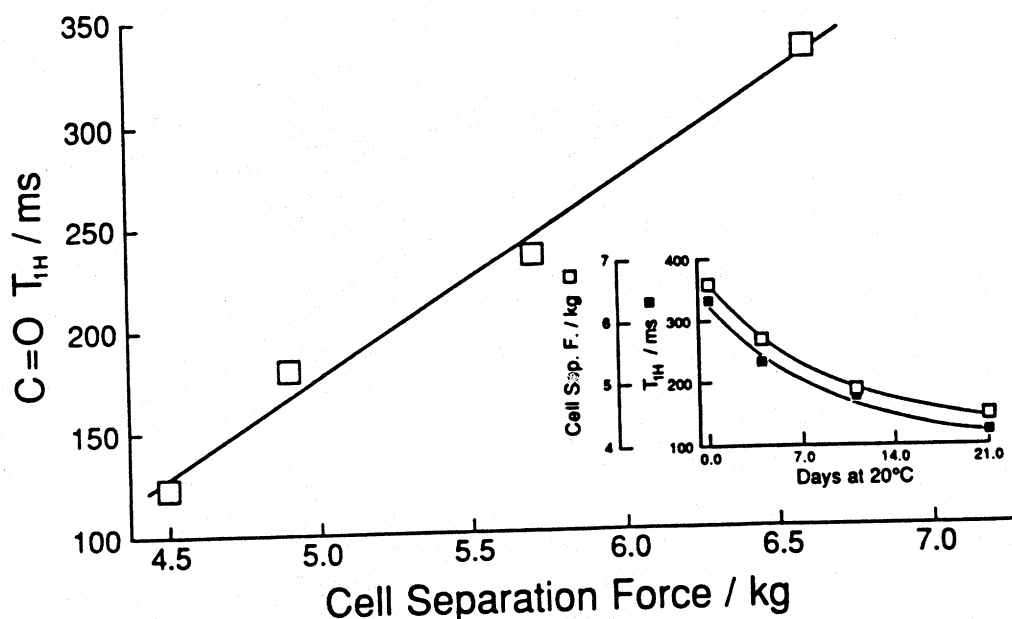


FIGURE 11. *Malus pumila* fruit ^1H spin-lattice relaxation time for the carbonyl resonance ($\text{C}=\text{O } T_{1H}$) and cell separation force as a function of ripening time at 20°C . At each time interval, stored fruit were randomly selected and cell separation force measured with an Instron Universal testing device equipped with a 0.79-cm (OD) plunger. Peak intensities were used for the calculation of $^{13}\text{C } T_{1\rho}$, $^1\text{H } T_{1\rho}$, as well as $^1\text{H } T_{1\rho}$ relaxation parameters by standard literature least square methods.³¹ SEs were calculated from the least squares analysis of all data. (From Irwin, P. L., Pfeffer, P. E., Gerasimowicz, W. V., Pressey, R., and Sams, C. E., *Phytochemistry*, 23, 2239, 1984.)

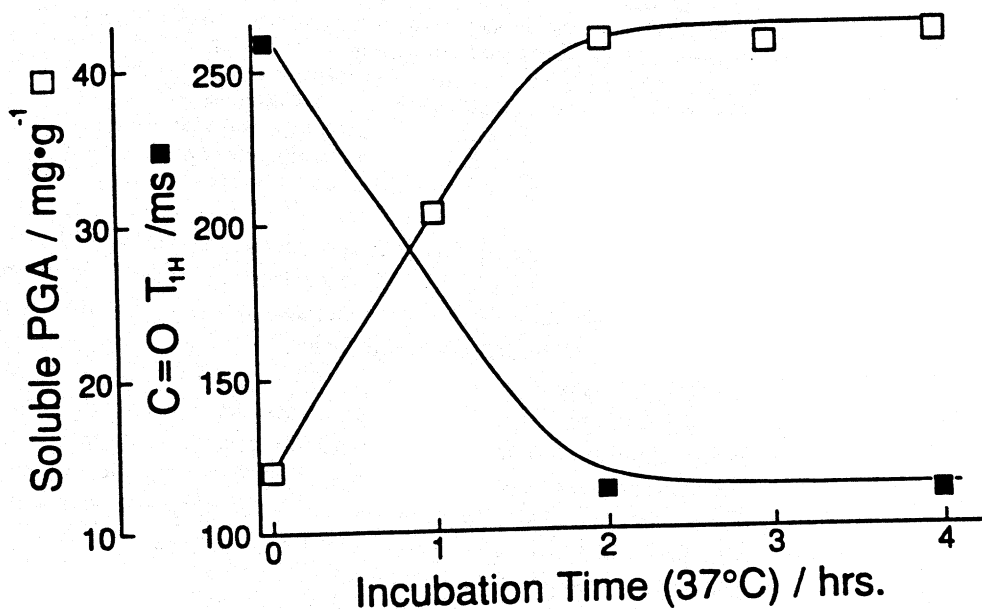


FIGURE 12. Changes in carbonyl ^1H spin-lattice relaxation times ($\text{C}=\text{O } T_{1H}$) and water soluble polyuronides (Soluble PGA) as a function of time at 37°C in the presence of tomato fruit PG II, an endo-cleaving polygalacturonase. Samples were dehydrated and critical point dried as noted previously. (From Irwin, P. L., Pfeffer, P. E., Gerasimowicz, W. V., Pressey, R., and Sams, C. E., *Phytochemistry*, 23, 2239, 1984.)

Table 2
¹H SPIN-LATTICE (T_{1H}) AND ROTATING FRAME SPIN-LATTICE (T_{1ρH}) RELAXATION TIMES DETERMINED FROM CARBONYL (δ_{C=O} = 172 PPM) AND/OR NONSPECIFIC RING CARBON (δ_{COH} = 74 PPM) RESONANCES IN INTACT APPLE CELL WALL SAMPLES AT DIFFERENT TIMES AT 20°C³

Days at 20°C	T _{1H} ± SE/ms		T _{1ρH} ± SE/ms	
	δ = 74 ppm	δ = 172 ppm	δ = 172 ppm	δ = 74 ppm
0	245 ± 3	4.3 ± 0.4	4.2 ± 0.2	—
4	142 ± 15	—	—	—
11	160 ± 4	4.6 ± 0.5	4.1 ± 0.2	—
21	207 ± 4	—	—	—

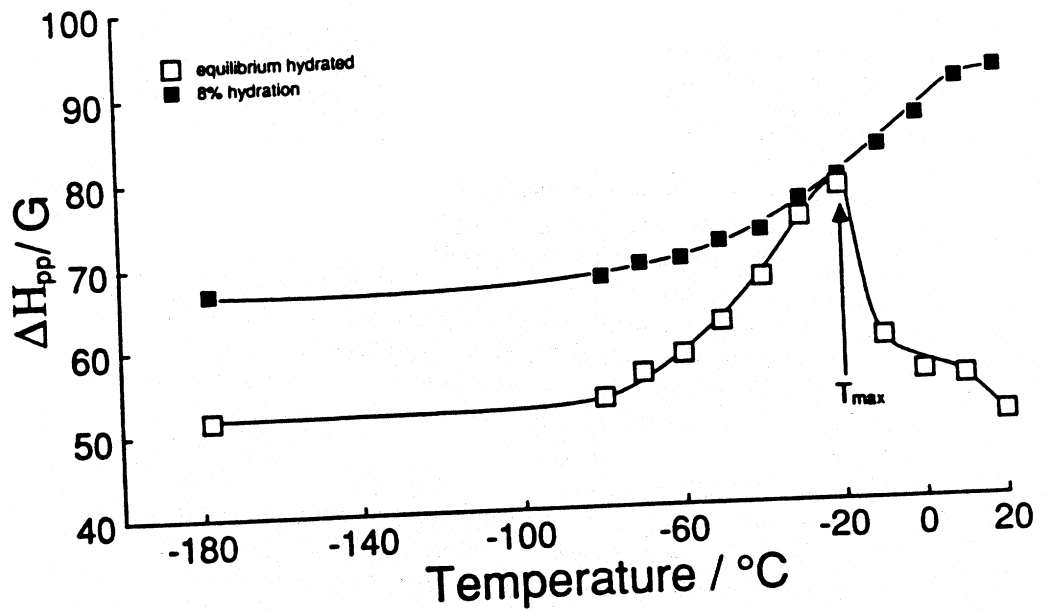


FIGURE 13. Temperature dependence of cell wall-bound Mn²⁺ line widths (ΔH_{pp}) for slightly hydrated (8% [w/w], closed squares) and equilibrium hydrated (about 70% [w/w], open squares) cell wall complex. Hydrated samples were prepared by equilibrating the critical point dried cell wall matrices various times (0.5 to 0.75, 1 to 1.5, 2 to 3, and 4 to 6 h for 21.7 ± 0.3, 32.9 ± 0.5, 42.0 ± 0.4, and 51.7 ± 0.5% [w/w] bound H₂O, respectively) in a saturated water vapor chamber at 160 torr and 22°C. (From Irwin, P. L., Sevilla, M. D., and Stroudt, C. L., *Biochim. Biophys. Acta*, 842, 76, 1985.)

function of sample temperature (Figures 13 and 14).⁶ In these studies, Mn²⁺-Mn²⁺ nearest neighbor distance parameters (d) were calculated as follows:

$$\Delta H_{pp} = 2 \left(\frac{3}{5} \cdot g^4 \beta^4 h^{-2} \cdot S(S+1) \cdot \frac{\kappa^2}{d^6} \right)^{1/2} \quad (3)$$

The constants g, β, and h have their usual values, and S represents the total electron spin of Mn²⁺. This calculation is based on the fact that the ΔH_{pp} for a Gaussian line is equal to two times

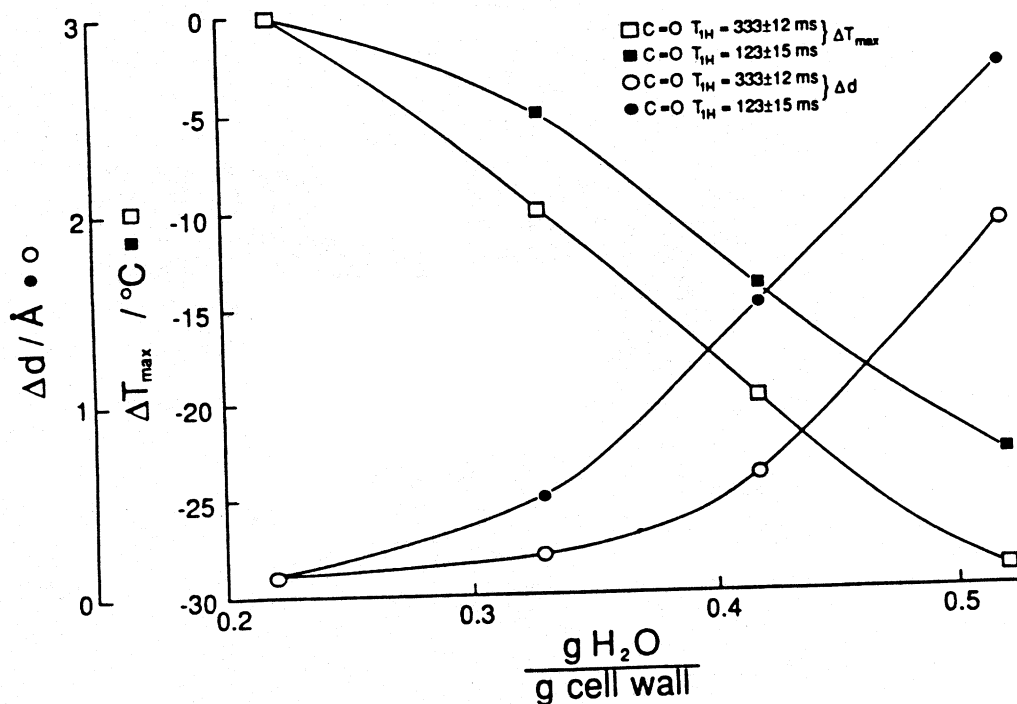


FIGURE 14. Dependence of Δd and ΔT_{max} on Mn^{2+} binding site-associated spin-lattice relaxation times ($C=O T_{1H}$) as a function of degree of cell wall hydration. Δd is the calculated change in d between $20^\circ C$ and T_{max} , assuming $k = 2.5$ throughout. This calculation assumes that all ΔH_{pp} perturbations were due to distance, as opposed to motional effects. (From Irwin, P. L., Sevilla, M. D., and Stroudt, C. L., *Biochim. Biophys. Acta*, 842, 76, 1985.)

the square root of the second moment.^{29,30} In Equation 3, d is the distance (in units of Å) between neighboring spins; κ (κ^2 is an approximation of the number of strong spin-spin interactions per point dipole), which is the lattice constant,⁶ depends on the arrangement of ions in the lattice, and is approximately one for a two spin system, $\sqrt{3}$ for a linear sequential array, and from $\sqrt{8}$ up to $\sqrt{12}$ for a three-dimensional hexagonal close packing array.^{4,6} It has been shown before that divalent cations bind to cell wall polyuronides in a spatially sequential fashion.^{4,6} As a consequence of this special case of cooperative ion binding, bound paramagnetic ion ΔH_{pp} are large, even at very low concentrations (Figure 9), due to their close spatial proximity to near neighbor paramagnetic species. In Figure 13 are shown cell wall bound Mn^{2+} ($1.89 \times 10^{-5} \text{ mol} \cdot \text{g}^{-1}$ = about 3 mol%) ΔH_{pp} as a function of sample temperature and degree of hydration. As the paramagnetic ion cell wall lattice approached equilibrium hydration, an unusual temperature dependency became apparent. The 20 and $-180^\circ C$ ΔH_{pp} were approximately equal; however, ΔH_{pp} increased to a maximum at about $-20^\circ C$ (T_{max}) and fell normally thereafter. Initially, it was thought that this maxima was due to a conformational change in polygalacturonan blocks as a consequence of the freezing of bound H_2O . However, further experiments (Figure 14) indicated that, as the degree of hydration increased, the T_{max} diminished and argues strongly against the ΔH_{pp} maxima being associated with the freezing of bound H_2O . For these calculations⁶ (ΔT_{max} , Figure 14), 320 ΔH_{pp} observations were made which encompassed several degrees of hydration, all temperatures (T), levels of bound Mn^{2+} ($[Mn]$) and 2 paramagnetic ion lattice structures (as represented by different $C=O T_{1H}$'s). All the ΔH_{pp} data were fit to a statistical model quadratic with respect to both $[Mn]$ and T . The partial first derivatives were taken with respect to T and $[Mn]$ and set to zero such that

$$\frac{\delta \Delta H_{pp}}{\delta T} = 0$$

$$a_1 T + b_1 [Mn] = c_1 \quad (4)$$

and

$$\frac{\delta\Delta H_{pp}}{\delta[Mn]} = 0$$

$$a_2T + b_2[Mn] = c_2 \quad (5)$$

T_{max} (T where $\partial\Delta H_{pp}/\partial T = 0$) values were then calculated by the method of simultaneous equations whereupon

$$T_{max} = \frac{\begin{vmatrix} c_1 & b_1 \\ c_2 & b_2 \end{vmatrix}}{\begin{vmatrix} a_1 & b_1 \\ a_2 & b_2 \end{vmatrix}} \quad (6)$$

ΔT_{max} is the change in T_{max} relative to the lowest level of hydration. These data demonstrate that the cell wall anionic polymer ligand structure affects the T_{max} as well as Δd , the calculated change in the Mn^{2+} near neighbor distance parameter between 20°C and T_{max} . Thus, during the approach to T_{max} , Mn^{2+} binding sites with a short C=O T_{III} conformationally flex about 0.7 ± 0.2 Å more than cell wall polygalacturonans of the corresponding treatment at equivalent levels of hydration.

IV. CONCLUSION

^{13}C CPMAS NMR, 1H broadline NMR, and EPR are useful in studying certain chemical and physical properties of plant cell walls and matrix polysaccharides. With specific ^{13}C or other specific isotopic labeling of cell wall components, solid-state NMR could be of even more utility, albeit at a great cost. However, problems associated with incomplete dehydration, paramagnetic ion-induced perturbations of relaxation behavior as well as nonrepresentative functional group 1H - ^{13}C polarization transfer should be addressed before interpretation of the data.

Various NMR relaxation time and EPR data clearly indicate that plant cell wall polygalacturonans increase in mobility or flexibility during the cell separation process and dissolution of the middle lamella.⁸ Such observations are important because of the noninvasive nature of these experiments. Most techniques for cell wall polysaccharide characterization provide little structural information about their behavior and arrangement within the matrix. Certain techniques could yield spurious results² due to the requisite extraction and solubilization processes possibly resulting in alterations of the polymer's primary and higher order structure.

The ^{13}C CPMAS NMR data reported herein could be interpreted as evidence for the specific action of an unidentified endo-cleaving polygalacturonan hydrolase.³ An exoPG, which produces monomers upon hydrolysis, should have resulted in an overall loss of C=O signal since the uronic acid monomer is soluble in most of the ethanol:H₂O solutions used to prepare these samples; this was not observed. Perturbations in polygalacturonan main chain flexibility could also be due to alterations in the structure of either pectin's neutral sugar fraction or some other near neighbor polymer species. However, in light of newer information²⁵ about the structural similarity of cell wall polygalacturonans during the cell separation process, the latter interpretation appears to be more likely.

REFERENCES

1. Hall, M. A., Cell wall structure in relation to texture, in *Quality in Stored and Processed Vegetables and Fruits*, Goodenough, P. W. and Atkin, R. A., Eds., Academic Press, London, 1981, 53.
2. Darvill, A., McNeil, M., Albersheim, P., and Delmer, D., The primary cell walls of flowering plants, in *The Biochemistry of Plants*, Vol. 1, Academic Press, New York, 1980, 91.
3. Irwin, P. L., Pfeffer, P. E., Gerasimowicz, W. V., Pressey, R., and Sams, C. E., Ripening-related perturbations in apple cell wall nuclear spin dynamics, *Phytochemistry*, 23, 2239, 1984.
4. Irwin, P. L., Sevilla, M. D., and Shieh, J. J., ESR evidence for sequential divalent cation binding in higher plant cell walls, *Biochim. Biophys. Acta*, 805, 186, 1984.
5. Irwin, P. L., Gerasimowicz, W. V., Pfeffer, P. E., and Fishman, M., ¹H-¹³C polarization transfer studies of uronic acid polymer systems, *J. Agric. and Food Chem.*, 1197, 1985.
6. Irwin, P. L., Sevilla, M. D., and Stoudt, C. L., ESR spectroscopic evidence for hydration- and temperature-dependent spatial perturbations of a higher plant cell wall paramagnetic ion lattice, *Biochim. Biophys. Acta*, 842, 76, 1985.
7. Irwin, P. L., Sevilla, M. D., Shieh, J. J., and Stoudt, C. L., Paramagnetic ion spin-spin coupling as direct evidence for cooperative ion binding to higher plant cell walls, in *Chemistry and Function of Pectin*, Fishman, M. L. and Jen, J. J., Eds., American Chemical Society, Washington, D.C., 1986, chap. 14.
8. Ben-Aire, R., Kislley, N., and Frenkel, C., Ultrastructural changes in the cell walls of ripening apple and pear fruit, *Plant Physiol.*, 64, 197, 1979.
9. Knee, M., Fruit softening. III. Requirement for oxygen and pH effects, *J. Exp. Bot.*, 33, 1263, 1982.
10. Morris, E. R., Physical probes of polysaccharides conformation and interactions, *Food Chem.*, 6, 15, 1980.
11. Bartley, I. M., β -Galactosidase activity in ripening apples, *Phytochemistry*, 13, 2107.
12. Havens, J. R. and Koenig, J. L., Applications of high-resolution carbon-13 nuclear magnetic resonance spectroscopy to solid polymers, *Appl. Spectrosc.*, 37, 226, 1983.
13. Schaefer, J. and Stejskal, E. O., High resolution C-13 NMR of solid polymers, *Top. in C-13 NMR Spectrosc.*, 3, 283, 1979.
14. Yannoni, C. S., High-resolution NMR in solids: the CPMAS experiment, *Acc. Chem. Res.*, 15, 201, 1982.
15. Pines, A., Gibby, M. G., and Waugh, J. S., Proton-enhanced NMR of dilute spins in solids, *J. Chem. Phys.*, 59, 569, 1973.
16. Irwin, P. L., unpublished data, 1985.
17. Alemany, L. B., Grant, D. M., Pugmire, R. J., Alger, T. D., and Zilm, K. W., Cross-polarization and magic angle sample spinning NMR spectra of model organic compounds. I. Highly protonated molecules, *J. Am. Chem. Soc.*, 105, 2133, 1983.
18. Alemany, L. B., Grant, D. M., Pugmire, R. J., Alger, T. D., and Zilm, K. W., Cross-polarization and magic angle sample spinning NMR spectra of model organic compounds. II. Molecules of low or remote protonation, *J. Am. Chem. Soc.*, 105, 2142, 1983.
19. Andrew, E. R., Bryant, D. J., and Cashell, E. M., Proton magnetic relaxation of proteins in the solid state: molecular dynamics of ribonuclease, *Chem. Phys. Lett.*, 69, 551, 1980.
20. Irwin, P. L. and Chamulitrat, W., unpublished data, 1987.
21. Anderson, D. M. W. and King, N. J., Polysaccharides of the Characeae. II. The carbohydrate content of *Nitella translucens*, *Biochim. Biophys. Acta*, 52, 441, 1961.
22. Anderson, D. M. W. and King, N. J., Polysaccharides of the Characeae. III. The carbohydrate content of *Chara australis*, *Biochim. Biophys. Acta*, 52, 449, 1961.
23. MacKay, A. L., Bloom, M., Tepfer, M., and Taylor, I. E. P., Broadline proton magnetic resonance study of cellulose, pectin and bean cell wall, *Biopolymers*, 21, 1521, 1982.
24. Knee, M. and Bartley, I. M., Composition and metabolism of cell wall polysaccharides in ripening fruits, in *Recent Advances in the Biochemistry of Fruits and Vegetables*, Friend, J. and Rhodes, M. J. C., Eds., Academic Press, London, 133, 1981.
25. Irwin, P. L., Sevilla, M. D., and Chamulitrat, W., Homopolygalacturonan molecular size in plant cell wall matrices via paramagnetic ion and nitroxyl amide dipolar spin-spin interactions, *Biophys. J.*, 54, 337, 1988.
26. Dilley, D. R., Enzymes, in *The Biochemistry of Fruits and their Products*, Hulme, A. C., Ed., Academic Press, London, 1970, 195.
27. Knee, M., Changes in structural polysaccharides of apples ripening during storage, in *Facteurs et Regulation de la Maturation des Fruits*, No. 238, Centre del la Recherche Scientifique, Paris, 1974, 341.
28. Cornell, B. A., Davenport, J. B., and Separovic, F., Low-frequency motion in membranes; the effect of cholesterol and proteins, *Biochim. Biophys. Acta*, 337, 689, 1982.
29. Van Vleck, J. H., The dipolar broadening of magnetic resonance lines in crystals, *Phys. Rev.*, 74, 1168, 1948.
30. Poole, C. P., *Electron Spin Resonance*, 2nd ed., John Wiley & Sons, New York, 1982, chap. 12.
31. Draper, N. and Smith, H., *Applied Regression Analysis*, 2nd ed., John Wiley & Sons, New York, 1981, chap. 1.

Chapter 12

SOLID-STATE NMR STUDIES OF TREATED WOOD AND LIGNIN

James F. Haw

TABLE OF CONTENTS

I.	Introduction	356
A.	Lignin Utilization	356
B.	CP/MAS NMR.....	362
C.	Low-Temperature Lignin Pyrolysis	365
D.	Kraft Pulping	369
II.	Conclusions	369
	References	369

I. INTRODUCTION

A. Lignin Utilization

After cellulose, lignin is the most abundant organic material on earth. It is a major constituent of all vascular plants and a major renewable source of reduced carbon. As such, lignin is potentially one of our most important raw materials. Most of the technology associated with lignin regards its elimination from wood in the production of paper. Approximately 200 million pounds/d of lignin are produced in the U.S. by the pulping of wood. Unfortunately, this potentially valuable resource is burned for its minimal heating value (2 to 3¢/lb) rather than using it as a starting material for more valuable products.

Possible useful products which could be made from lignin include fuels, fertilizers, adhesives, surfactants, and dispersants. Extensive reviews of the structure and chemistry of lignin have been published elsewhere.¹ Many processes used to treat wood or lignin involve selected reagents including various alkaline or acidic catalysts, oxidative or reductive reagents, or selected modifiers used to make copolymers. While these processes have diverse approaches, they either depolymerize lignin into smaller and more useful compounds or modify the lignin to form polymeric or copolymeric materials.

B. CP/MAS NMR

The development of new strategies for the utilization of lignin will depend, in part, on the availability of analytical techniques for characterization of the complex materials produced by such strategies. A number of investigators, especially Nimz and co-workers have demonstrated^{2,4} the value of solution state ¹³C-NMR for studies of soluble lignin fractions. Its applicability, however, is limited by the necessity of modifying or degrading the sample to obtain a soluble fraction. Fortunately, in the last decade, it has become possible to obtain high-resolution ¹³C-NMR spectra of solid samples.^{5,7} This is possible through a combination of technical advances designed to overcome the line-broadening effects and sensitivity problems that formerly precluded high-resolution studies of typical solids. The first technique is high-power proton decoupling which is used to eliminate a major line-broadening interaction due to dipole-dipole coupling between ¹³C and the protons in the sample. A double-resonance experiment called cross-polarization (CP) is used to increase the intrinsic sensitivity of ¹³C and to increase the rate at which the signal can be time averaged.

In addition to the above techniques, which involve high-power radio frequency pulses, the sample is usually rotated about a particular angle, called the magic angle, which is 54.7° from the direction of the magnetic field, B_0 . This angle is important because many of the line-broadening interactions in NMR depend on the geometric term $3\cos^2\Theta - 1$, and this term has a value of zero when Θ is selected to be the magic angle. When the sample is spun very rapidly (i.e., 4 kHz = 240,000 rpm) about an axis inclined at the magic angle, the line broadening due to chemical shift anisotropy (CSA) is removed. If high-power proton decoupling is also used, high-resolution ¹³C spectra of solids may be observed. CP is normally used with the other techniques, and the complete experiment is called the CP/MAS experiment.

The chemical shifts observed in CP/MAS experiments are essentially identical to those observed in solution. Confirmation of structural assignments for CP/MAS spectra is facilitated by variants of the basic CP/MAS experiment that select particular structural units for observation. The most important example of such assignment aids is the interrupted-decoupling experiment⁸ which provides spectra with signals from quaternary carbons and methyl carbons exclusively. With spectra such as these, detailed assignments are possible and the modification of lignin or wood samples by thermal and/or chemical means can be monitored without the complication and uncertainty of further modification for the purpose of solubility.

In the last several years, there have been a number of reports of the use of ¹³C-CP/MAS NMR to characterize plant materials and the effects of various treatment processes on plant materials.

^{13}C -CP/MAS NMR has been used for the characterization of wood,^{9,11} steam exploded wood,¹⁰ steam hydrolyzed wood,¹² wood pulps,¹¹ herbaceous plants,¹³ seeds,^{14,15} pyrolyzed wood,¹⁶ model sludge components,¹⁷ lignin,^{18, 19} cellulose^{20,22} and autohydrolyzed wood.²³ In the last-cited study it was possible to quantify the lignin and to estimate the hemicellulose remaining in the solid products of four biomass treatment processes, on the basis of the ^{13}C -CP/MAS NMR spectra of those products. It has been shown that quantitative, as well as qualitative information about lignin composition is obtained from ^{13}C -CP/MAS studies.¹¹ Further details of the CP/MAS experiment and its application to plant constituents may be found in other chapters of this volume.

^{13}C -CP/MAS NMR has recently proved to be a highly informative method for the study of lignins and other solids obtained from wood treatment processes. This is illustrated in the remainder of this chapter which summarizes some of the results of three studies: rapid steam hydrolysis (RASH) of red oak,¹² low temperature lignin pyrolysis,¹⁶ and the kraft pulping process.¹¹ RASH treatment has been selected as a representative process for the partial depolymerization of lignin. Although pyrolysis is not likely to produce useful products from lignin, its study is important in that most treatment processes involve heat treatment in presence of selected reagents, and it is useful to understand the effects of heat alone in sorting out the roles of solvent, heat, and added reagents. The effects of kraft pulping on the lignin spectra have been studied because this process represents an important industrial source of lignin, and the properties of kraft lignins are, therefore, of great interest.

Rapid steam hydrolysis²⁴ (RASH) is similar to steam explosion in that wood chips are subjected to high-pressure steam at temperatures in the range of 200 to 280°C in both processes. The RASH process differs from the steam explosion process in that no sudden decompression is used in the former process. The RASH process also involves the continuous introduction of steam during the treatment period, with volatile and water-soluble products (principally depolymerized hemicellulose and depolymerized lignin) continuously removed from the reactor and recovered with the steam condensate. One advantage of the RASH process is that cellulose recovery is somewhat better than with steam explosion under similar conditions, presumably due to the continuous removal of acetic acid in the RASH process.

All of the ^{13}C -NMR spectra in this chapter were obtained at 25.27 MHz with a home-built spectrometer at Colorado State University. The pulse repetition time was 1 s and the CP contact time was 1 ms. The ^1H irradiation field was 12 G, and 1-K data points were zero-filled to 4-K points. Sleeve-type bullet spinners with sample volumes of 0.4 cm³ were used and were spun at approximately 3.5 kHz. Chemical shifts were measured with respect to tetramethylsilane via hexamethylbenzene as a secondary substitution reference (aromatic peak at 132.3 ppm). A total of 12,000 to 40,000 scans were accumulated for each spectrum.

To a first approximation, wood is a mixture (or possibly a copolymer) of lignin, cellulose, and noncellulosic polysaccharides, termed hemicellulose. The principal repeat units of conifer lignin are derivatives of guaiacylpropane, I. Hardwood lignins also contain repeat units derived from syringylpropane (Structure I with a second methoxy group at position 5). The anhydroglucose repeat unit (Structure II) of cellulose is also shown.

Figure 1a is the ^{13}C -CP/MAS spectrum of ground, untreated red oak wood. This spectrum is qualitatively similar to spectra of pine wood^{9,11} and ash wood¹⁰ for which spectral assignments have recently been made. Drawing on the work in those previous studies, peak assignments can be made for the spectrum in Figure 1a as described below.

The peak at 172 ppm is principally due to the carbonyl carbons of acetyl groups and carboxylic acid groups in hemicellulose. The region between 160 ppm and 143 ppm consists primarily of signals due to the oxygen-substituted aromatic carbons of lignin. There are two partially resolved signals in this region, a more-intense signal at 153 ppm and a less-intense signal at 148 ppm. The 153-ppm signal is prominent in the spectrum of ash wood, but is of much

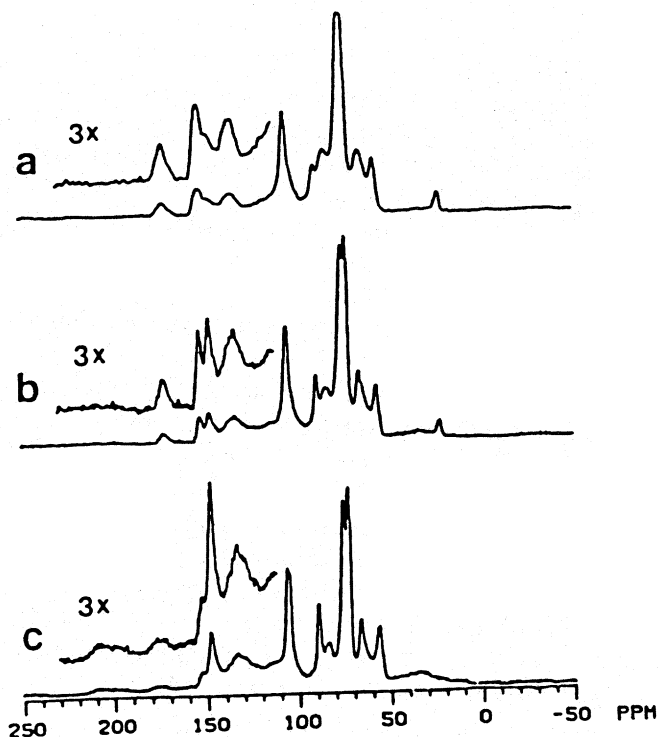
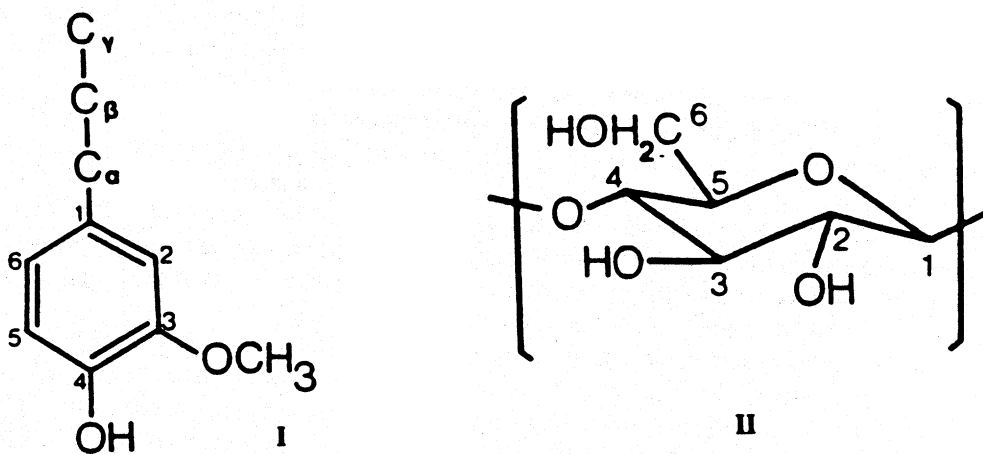


FIGURE 1. ^{13}C -CP/MAS NMR spectra of red oak wood: (a) untreated red oak, (b) red oak subjected to RASH treatment at 230°C for 1.5 min, and (c) red oak subjected to RASH treatment at 270°C for 1 min. (From Haw, J. F., Maciel, G. E., and Biermann, C. J., *Holzforschung*, 38, 327, 1984. With permission.)



lower intensity in the spectra of pine wood samples. On that basis alone, it is reasonable to assign the 153-ppm peak to one or more of the carbons in syringyl units, since the presence of syringyl units in hardwood lignin but not in softwood lignin is a major compositional difference between these two lignins. The relative intensity of the 153-ppm signal is not dramatically reduced in an interrupted-decoupling experiment indicating that this signal is primarily due to nonprotonated carbons (interrupted-decoupling spectrum not shown). A more definitive assignment of the 153-ppm peak can be made on the basis of a previously reported liquid-solution ^{13}C -NMR study³ of a large number of dimeric and monomeric lignin model compounds. The only ^{13}C -NMR signals observed in that previous study in the 151- to 157-ppm region that were assigned to nonpro-

Table 1
¹³C-NMR SPECTRAL ASSIGNMENTS FOR
HARDWOOD LIGNINS

Chemical shift (range) (ppm)	Assignment
210—190	Aldehyde and ketone carbonyls
180—166	Ester carbonyls
153	S3/5(4-O-R)
148	S3/5(4-O-H), G3/4
137	S1/4(4-O-R), G1(4-OH)
134	S1/4(4-O-H), G1(4-OH)
120	G6
115	G5
112	G2
106	S2/6
84	C-β in β-0-4
74	C-α-OH in β-0-4
60	C-γ-OH
52—15	Aliphatic C not bound to oxygen

Note: G, guaiacyl; S, syringyl.

tonated carbons were assigned to C-3 and C-5 of syringyl units that are O-alkylated at C-4 (154 ppm), and C-4 of guaiacyl units with a ketone group at the α position on the propyl chain (152 ppm). Ludemann and Nimz also studied³ the liquid-solution ¹³C-NMR spectrum of the milled-wood lignin obtained from beech and reported that for that material the signal assigned to C-3 and C-5 of O-alkylated syringyl units was much more intense than the signal assigned to C-4 of guaiacyl units with a ketone group at the α position. On that basis, the signal at 153 ppm in Figure 1a is assigned primarily to C-3 and C-5 of syringyl units O-alkylated at C-4. The abundance of O-alkylation at C-4 in red oak lignin implied by this assignment for the spectrum in Figure 1a is hardly surprising; aryl-alkyl ether linkages involving C-4 are firmly established as a major linkage in lignin.¹

The spectral region in Figure 1a between 150 ppm and 142 ppm consists of signals due to the oxygen-substituted aromatic carbons of a number of guaiacyl and syringyl derivatives, including C-3 and C-5 of syringyl units which are not alkylated at C-4.³ The signal intensity in Figure 1a between 143 and 130 ppm is primarily due to C-1 carbons of guaiacyl and syringyl groups, but several other carbon-types, including C-4 of nonalkylated syringyl groups, also contribute intensity to this region.³ The intensity between ~130 and ~110 ppm in Figure 1a is primarily due to C-2, C-5, and C-6 of guaiacyl units. Signal intensity due to C-2 and C-6 of syringyl units will be assigned on the basis of the spectrum of HC1 lignin from red oak (*vide infra*).

The remaining features in Figure 1a are assigned as follows. The signal at 57 ppm is due to methoxy groups, principally those of lignin. The signal at 22 ppm is assigned to the methyl carbon of acetyl groups in hemicellulose. The low-intensity signals in the region from 50 ppm to 27 ppm are assigned to alkyl carbons not attached to oxygen, such as certain carbons found in the propyl chains in lignin and in extractives. Representative spectral assignments are summarized in Table 1.

Having presented a detailed assignment of the spectrum of untreated red oak, we now consider the effects of RASH treatment on red oak, as reflected in the spectra of the resulting solid products. Figure 1b is the ¹³C-CP/MAS NMR spectrum of the solid residue obtained by RASH treatment of red oak at 230°C for 1.5 min. In the absence of an internal standard, it is not easy to directly compare the absolute intensities of signals in one spectrum to those in another spectrum. However, it is possible to make comparisons of relative intensities obtained from

different spectra. The intensity assigned to the methyl carbon of the acetyl group at 22 ppm in Figure 1b relative to the other signals in that spectrum is only ~30% lower than the corresponding relative intensity in Figure 1a (untreated red oak). This result indicates that the generation of acetic acid by the action of steam on hemicellulose is slow for red oak chips at 230°C. Evidence for the partial removal of hemicellulose is provided by the reduction of the ratio of peak heights at 84 and 89 ppm from 1.3 in the spectrum of untreated red oak wood (Figure 1a) to 0.82 in the spectrum of the 230°C RASH solids (Figure 1b). The 84-ppm/89-ppm peak-height ratio has been previously applied as a convenient semi-quantitative indicator of the removal of hemicellulose in biomass treatment processes.²³ Further spectroscopic evidence for the reduced hemicellulose content in the 230°C RASH solids is afforded by the substantial increase in the splitting of the two signals at 75 ppm and 73 ppm. These signals are due to cellulose, and their resolution can be degraded by the presence of hemicellulose, which is known to contribute intensity between these signals.⁹

A very significant difference between the spectrum of the 230°C RASH solids (Figure 1b) and the spectrum of the untreated wood (Figure 1a) is the change in the relative intensities of the 153-ppm and 148-ppm peaks. RASH treatment at 230°C decreases the relative intensity of the 153-ppm peak while increasing the relative intensity of the 148-ppm peak. Based on the assignments of these peaks (*vide supra*), these data clearly show that RASH treatment at 230°C partially depolymerizes red oak lignin by hydrolyzing the aryl-alkyl linkages involving C-4 of syringyl units. Other transformations of the lignin are also likely, but these cannot be identified conclusively on the basis of the spectra in Figures 1a and b. For example, dealkylation of a guaiacyl unit will shift its liquid-solution C-4 resonance from 150 ppm to 147 ppm,³ but this change is not clearly evident in Figures 1a and 1b, possibly because of overlap with signals from other components.

Hydrolysis of aryl-alkyl ether linkages is even more apparent in the ¹³C-CP/MAS NMR spectrum of the solids obtained by a 1-min RASH treatment at 270°C (Figure 1c). The relative intensity of the 153-ppm signal is substantially reduced in Figure 1c relative to Figures 1a and b, with a corresponding substantial increase in the 148-ppm signal. This result indicates that substantial hydrolysis of aryl-alkyl ether linkages is achieved by RASH treatment at 270°C. The increase in the relative intensities of the aromatic signals following RASH treatment at 270°C is at least in part due to the preferential removal of carbohydrates (principally hemicellulose) with the steam condensate, resulting in a concentration of the lignin in the RASH solids.

The 84-ppm/89-ppm peak-height ratio is only 0.75 in Figure 1c (relative to the ratio 1.3 in Figure 1a), a result consistent with significant removal of hemicellulose. Removal of hemicellulose with these conditions has been previously demonstrated on the basis of wet-chemical analysis.²⁴ The methyl carbon signal of the acetyl group (22 ppm) is completely absent in Figure 1c. The ¹³C spectrum in the region between 112 ppm and 60 ppm in Figure 1c is very similar to the corresponding region of previously-reported spectra of cellulose I.^{20,22}

Figure 1c also shows low-intensity carbonyl signals. The very broad signal between 220 ppm and 190 ppm is assigned to aldehyde and ketone groups, which are probably associated with lignin. The peak between 170 and 183 ppm is characteristic of esters and carboxylic acids. Since Figure 1c shows no evidence of hemicellulose, the esters and/or carboxylic acid groups are probably associated with lignin.

It has been demonstrated previously²⁴ that some lignin appears in the steam condensate during RASH treatment at temperatures above 210°C. A lignin fraction was obtained by filtration of the steam condensate from the 270°C run and subjected to NMR analysis. To serve as a basis of comparison, a ¹³C-CP/MAS spectrum of the HCl lignin²⁵ obtained from red oak was acquired (Figure 2a). HCl lignin is believed to be much more similar to native lignin than is Klason lignin, which is highly condensed and unreactive. Figure 2a has features which are similar to the features assigned to lignin in the spectrum of untreated red oak wood (Figure 1a). In particular, the peak at 153 ppm is more intense than the peak at 148 ppm, indicating that the HCl lignin has a substantial amount of aryl-alkyl ether linkages. Figure 2a also shows

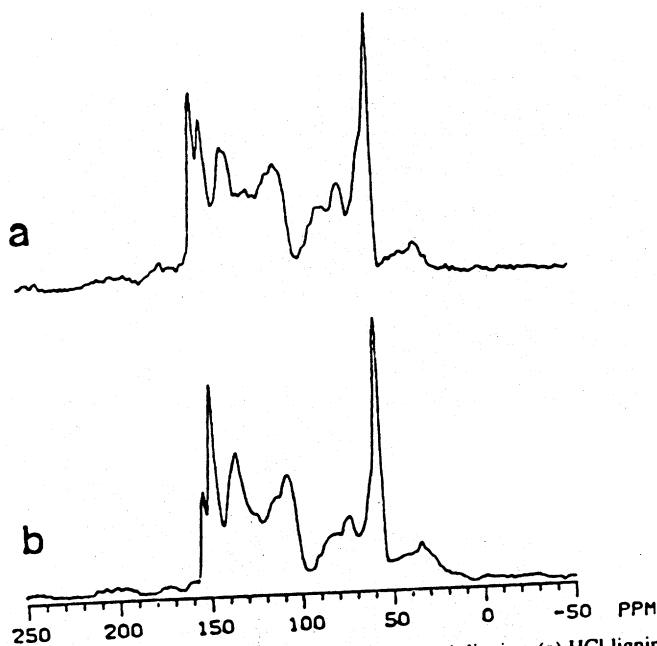


FIGURE 2. ^{13}C -CP/MAS NMR spectra of red oak lignins: (a) HCl lignin derived from red oak, and (b) solids obtained from steam condensate following RASH treatment of red oak at 270°C for 1 min. (from Haw, J. F., Maciel, G. E., and Biermann, C. J., *Holzforschung*, 38, 327, 1984. With permission.)

significant intensity in the 110 ppm to 103 ppm region, which can be attributed to C-2 and C-6 of syringyl units on the basis of the liquid-solution work of Ludemann and Nimz.³ This intensity is masked in Figures 1a to c by overlap with the intense signal due to C-1 of cellulose (105 ppm).

The peaks at 83 and 74 ppm in Figure 2a are due to oxygen-substituted aliphatic carbons. It is not clear on the basis of Figure 2a whether these signals are due to lignin or to a small amount of carbohydrates. The peak at 56 ppm in Figure 2a is due to methoxy groups. The 61-ppm shoulder on this peak is significantly attenuated in an interrupted decoupling experiment. These data suggest that the 61-ppm shoulder peak is due to an oxymethylene group. Figure 2a also shows low-intensity aliphatic and carbonyl signals similar to those observed in the spectrum of the 270°C RASH solids (Figure 1c).

The ^{13}C -CP/MAS spectrum of the lignin obtained from the steam condensate of the 270°C RASH treatment is presented in Figure 2b. Comparison of Figure 2b with Figure 2a (HCl lignin) reveals differences consistent with the steam condensate lignin being significantly more depolymerized than is HCl lignin. In particular, compared with the patterns seen for the HCl lignin (Figure 2a), the 153-ppm signal in Figure 2b is of reduced relative intensity, while the relative intensity of the 148-ppm signal is increased. These results show that the aryl-alkyl ether linkages have been extensively hydrolyzed in the formation of steam condensate lignin. This result was also observed for the lignin remaining in the RASH solids (*vide supra*).

This study has shown that ^{13}C -CP/MAS NMR can characterize the extent of aryl-alkyl ether hydrolysis in hardwood lignins during biomass treatment by steam hydrolysis. This is possible because several of the carbons in syringyl and guaiacyl groups have chemical shifts which differ significantly (3- to 5-ppm differences) on the basis of whether or not C-4 is alkylated. The effect is most clearly seen for C-3 and C-5 of syringyl units, which give a single well-resolved peak at 153 ppm when C-4 is alkylated, while the corresponding resonance is at 148 ppm when the aryl-alkyl ether linkage is cleaved.

On the basis of interrupted decoupling experiments and the liquid-solution ^{13}C -NMR work of Ludemann and Nimz, it is possible to make a fairly detailed assignment of the ^{13}C -CP/MAS spectra of red oak lignins. The close agreement between the liquid-solution chemical shifts of

lignin model compounds reported in that previous study and the solid-state chemical shifts observed for lignin in the present study is satisfying.

C. Low-Temperature Lignin Pyrolysis

Recently, the application of ^{13}C -CP/MAS NMR to the study of low-temperature pyrolysis of two lignins derived from sweetgum has been reported.¹⁶ In that work, ^{13}C -CP/MAS NMR, FT-IR, elemental analysis, and thermogravimetric analysis (TGA) were used to study the low temperature pyrolysis of steam exploded and HCl lignin from sweetgum. It was possible to deduce a variety of changes in the lignins as a result of pyrolysis. One-gram samples of lignin were pyrolyzed for 2 min in a pyrex tube immersed in a sand bath at various temperatures under a flowing nitrogen atmosphere. ^{13}C -CP/MAS spectra of the pyrolyzed HCl sweetgum lignins are shown in Figure 3. Analogous spectra for pyrolyzed steam exploded sweetgum lignins are shown in Figure 4. Chemical shift assignments for these spectra are summarized in Table 1. The changes in these NMR spectra features upon pyrolysis provide insight into the pyrolysis process.

^{13}C -CP/MAS spectra of three representative HCl lignin samples are presented in Figure 3. Figure 3a is the spectrum of the unpyrolyzed material. The ^{13}C -CP/MAS spectrum of HCl red oak lignin was discussed previously. The changes of several of these spectra features upon pyrolysis provide important insight into the changes in the solid residues during lignin pyrolysis (Figures 3b and 3c). The intense peak at 153 ppm in Figure 3a is due to C-3 and C-5 of syringyl units involved in ether linkages at C-4 (principally β -0-4). The less intense peak at 148 ppm in Figure 3a is also due to C-3 and C-5 of syringyl units, but only for those with a free phenolic group at C-4. The relative intensities of these two signals can be used as a measure of the degree to which β -0-4 linkages are cleaved during the processing of wood, as was done in the steam hydrolysis study. The relative intensities of these peaks in Figure 3a indicate that the majority of syringyl units in unpyrolyzed HCl lignin are involved in ether linkages. Comparison of Figure 3a with the spectrum of pyrolyzed HCl lignin (Figures 3b, 250°C; Figure 3c, 280°C) reveals that these linkages are readily cleaved under the low-temperature pyrolysis conditions.

The peaks in Figure 3a at 84 ppm and 74 ppm and the shoulder at 60 ppm are due to aliphatic carbons bound to oxygen. For the alkyl chain of a β -0-4 syringylglycerol ether unit, these assignments correspond to C- β , C- α , and C- γ , respectively. It was possible to assign these signals to lignin, because a glucose analysis procedure revealed that the cellulose contents of these materials were low.¹² Comparison of Figure 3a with the pyrolyzed HCl lignin spectra (Figure 3b, 3c) suggests that dehydration of the alkyl chains occurs readily in lignin pyrolysis. This is evidenced by a reduction in the intensities of the peaks at 84 ppm and 74 ppm as a result of pyrolysis. The 60-ppm shoulder, although not as well resolved as in Figure 3a, is still present in Figures 3b and 3c, suggesting that primary alcohols are still present in lignin chars after pyrolysis at 280°C.

Comparing the 52 ppm to 15 ppm regions in the three spectra of Figure 3, one notes an increase in the number of aliphatic carbons not adjacent to oxygen (Table 1) in the residue as a result of pyrolysis. This is consistent with alkyl chain dehydration, provided that the alkenes formed in such dehydration reactions react rapidly under pyrolysis conditions to give alkyl chains. The formation of alkenes and carbonyls in lignin pyrolysis has been previously proposed on the basis of model compound studies.^{26,27}

The ^{13}C -NMR spectra in Figure 3 show that the accumulation of carbonyl functionality in the HCl lignin pyrolysis residues is very limited, in contrast to the results obtained in the previously reported model compound studies.^{26,27} The peak intensities between 210 ppm and 166 ppm in Figures 3b and 3c (pyrolyzed HCl lignin) are only slightly higher than in the spectrum of the unpyrolyzed material (Figure 3a). This observation suggests that most carbonyl functionality, if formed in lignin pyrolysis, is efficiently lost as volatile species. The evolution of formaldehyde and carbon dioxide during the pyrolysis of kraft lignin has been previously noted in an FT-IR evolved gas study.²⁸ The constant relative intensity of the methoxy carbon signal (56 ppm) in Figure 3 indicates that this group is stable over the temperature range of our study.

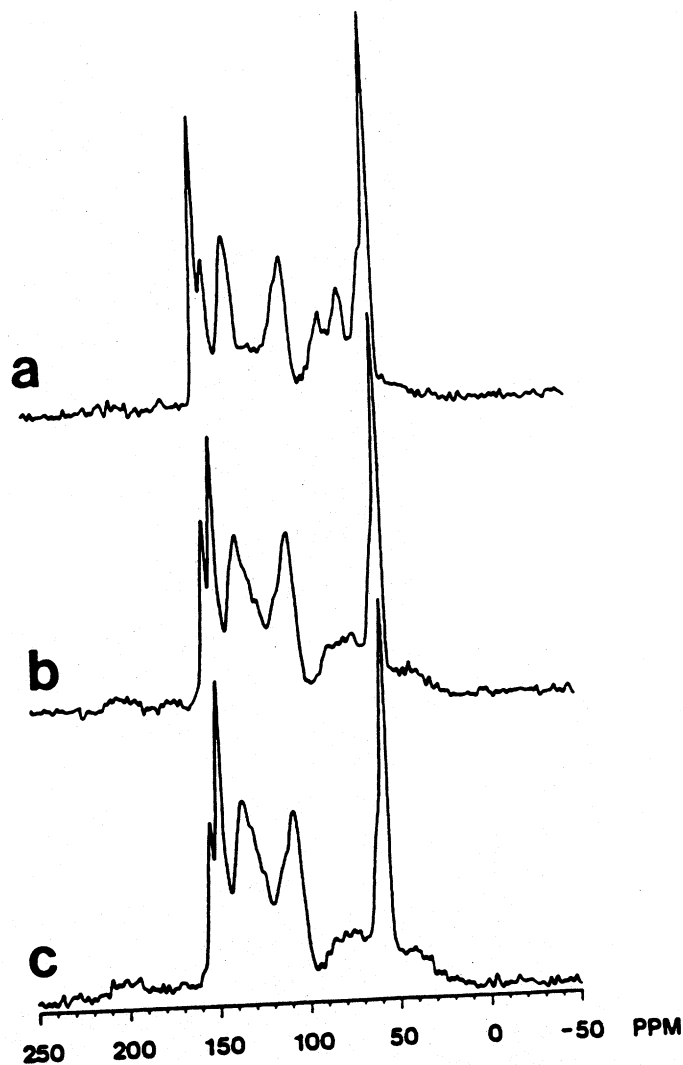


FIGURE 3. ^{13}C -CP/MAS NMR spectra of the HCl lignin obtained from sweetgum: (a) unpyrolyzed, (b) pyrolyzed at 250°C , and (c) pyrolyzed at 280°C . (From Haw, J. F. and Schultz, T. P., *Holzforschung*, 39, 289, 1985. With permission.)

The spectra in Figure 3 show that no major reorganization of the aromatic ring structures occurs at or below 280°C on the time scale of our pyrolysis experiment (2 min). The spectral changes in the aromatic regions (160 ppm to 100 ppm) of Figure 3 can be accounted for by ether cleavage alone, without recourse to cracking mechanisms or ring fusion.

^{13}C -CP/MAS NMR spectra of the samples obtained by pyrolyzing HCl lignin at 300 , 325 , and 335°C , respectively (not shown), follow the trend shown for pyrolysis at 250 and 280°C (Figure 3). In particular, the 153-ppm peak is barely visible as a shoulder in the spectrum of the 335°C pyrolysis product.

The above observations for HCl lignin pyrolysis largely apply to the results obtained for the steam-exploded lignin. Figure 4 shows the ^{13}C -CP/MAS NMR spectra of unpyrolyzed steam-exploded lignin (Figure 4a) and the residues of its pyrolysis at 250°C (Figure 4b) and 280°C (Figure 4c). The several differences between the spectra in Figure 4 (steam-exploded lignins) and Figure 3 (HCl lignins) are more a matter of degree than of kind. For example, the spectrum of the unpyrolyzed steam-exploded lignin (Figure 4a) shows a greater extent of ether cleavage than does the spectrum of the unpyrolyzed HCl lignin (Figure 3a). This effect is due to steam hydrolysis, as was observed in the ^{13}C -CP/MAS NMR study of the rapid steam hydrolysis of re-

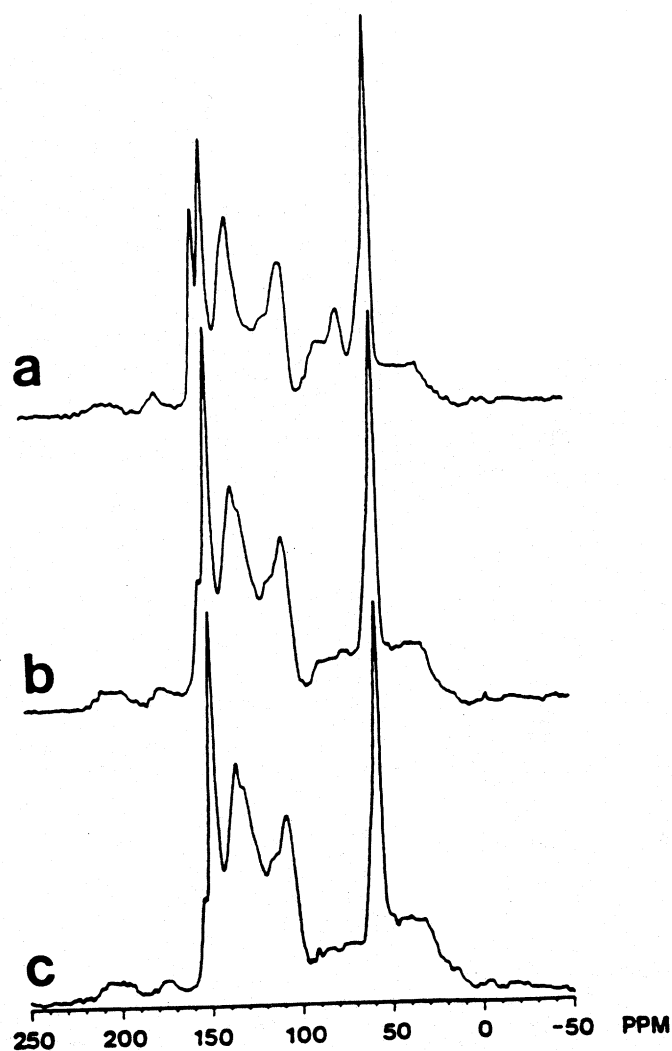


FIGURE 4. ^{13}C -CP/MAS NMR spectra of the lignin obtained from steam-exploded sweetgum: (a) unpyrolyzed, (b) pyrolyzed at 250°C , and (c) pyrolyzed at 280°C . (From Haw, J. F., and Schultz, T. P., *Holzforschung*, 39, 289, 1985. With permission.)

oak (*vide supra*, Section II.A). The trends observed in the pyrolysis of the steam-exploded lignin (Figure 4), however, are identical to those for HCl lignin (Figure 3). These same trends are also evident in the ^{13}C -CP/MAS NMR spectra of the samples obtained by pyrolyzing steam-exploded lignin at 220 and 235°C , respectively (not shown).

In conclusion, ^{13}C -CP/MAS NMR spectra provide fairly detailed insight into the structural changes of the residue (char) obtained in low-temperature lignin pyrolysis. These structural changes may be summarized by the following observations.

1. Aryl-alkyl ether linkages are extensively cleaved in the pyrolysis residue.
2. Dehydration of the alkyl chains occurs, approximately in parallel with ether cleavage.
3. Nonoxygen-substituted aliphatic material accumulates in the residue, possibly due to the condensation of alkenes initially formed in the dehydration step.
4. Carbonyl-containing species do not accumulate in the solid residue.
5. Methoxy groups are not cleaved below 335°C .

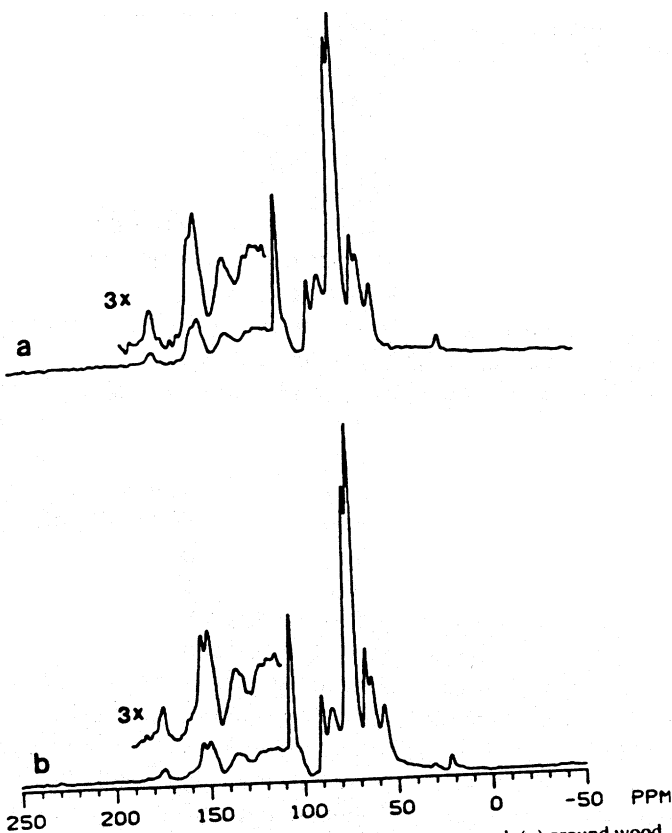


FIGURE 5. ^{13}C -CP/MAS spectra of southern pine wood: (a) ground wood, and (b) extractives-free wood.

6. No major reorganization of the aromatic rings (other than aryl-alkyl ether cleavage) occurs below 335°C in the residue.

Furthermore, the value of ^{13}C -CP/MAS NMR in the study of lignin pyrolysis has been demonstrated.

D. Kraft Pulping

The most important chemically modified wood product, wood pulp, has been produced commercially since the mid nineteenth century, when chemical pulping replaced mechanical pulping. Important processes in pulping include delignification and fiberization. Pulp production in the U.S. alone is on the order of 5×10^7 tons per year.

All pulp samples¹² were prepared in a 10-l electrically heated stainless steel rotating digester. All preparations used 1000 g of an oven-dried equivalent of air-dried loblolly pine (*Pinus taeda* L.) woodchips and a liquor-to-wood ratio of 4.5 (w/w). The digester was evacuated with a water aspirator for 20 min after it was filled (with the exception of the acid sulfite cook), but prior to starting the heating. The kraft cooks were carried out with 20% active alkali and 25% sulfidity (194 g of NaOH, 63 g of Na_2S). Three kraft pulps were prepared with various cook times. The lignin contents of these pulps (as determined by Kappa number or permanganate number) were: kraft 1, 14.5%; kraft 2, 4.3%; kraft 3, 2.2%.

Figure 5 shows the 25-MHz ^{13}C -CP/MAS spectra¹³ of ground southern pine wood (Figure 5a) and extractives-free southern pine wood (hereafter referred to as extractives-free wood, Figure 5b). Wood extractives constitute a diverse collection of materials, including phenols, terpenes, and resin acids. Comparison of Figure 5a and Figure 5b shows that the extractives contribute

some intensity to various regions of the pine wood spectrum. Since pulping removes most extractives, the extractives-free wood spectrum will be the basis of comparison used here for exploring modification of the lignin and carbohydrate fractions of wood in pulping.

¹³C-CP/MAS spectra of pine wood were assigned by Kolodjeski and co-workers.⁹ The assignments offered here are somewhat more detailed and form the basis for comparison with spectra of wood pulps. The intensity in the spectral region from 160 ppm to 110 ppm in Figure 5b is due to the aromatic ring carbons of lignin. The intensity between ~160 ppm and ~143 ppm is specifically due to oxygen-substituted aromatic ring carbons (e.g., carbons 3 and 4 in structure 1). The signals due to carbon types, α , β , and γ are overlapped with signals due to the carbohydrate components of wood and are not generally resolved. The signal at 56 ppm is due to methoxy carbons, principally of lignin, although approximately 10% are known from previous work²⁹ to be methoxy groups in some of the less common monomer units of hemicellulose, specifically the glucuronic acid in xylan.

The single peak at 105 ppm in Figure 5b is assigned to the C-1 carbon of the anhydroglucose repeat unit, 2. The sharper signal at 89 ppm and the broader high-shielding shoulder at 84 ppm are due to cellulose carbon C-4. The apparent doublet in the 70- to 80-ppm region is due to the C-2, C-3, and C-5 carbons. The peak at 66 ppm and shoulder at 63 ppm are due to the C-6 carbon of cellulose. These features are characteristic of cellulose I, the native (natural) form of cellulose. ¹³C-CP/MAS spectra of hemicellulose preparations have also been reported.⁹ Many of the spectral features are similar to those of cellulose, although the hemicellulose signals tend to be broader, reflecting the heteropolymeric nature of hemicellulose and the severity of the isolation procedures. Figure 5b shows three resolved signals that are readily assignable to hemicellulose. The broad, poorly resolved signal at 103 ppm (visible as a shoulder on the high-shielding side of the 105 ppm peak) is due to hemicellulose carbons that are structurally analogous to cellulose carbon C-1. The signals at 22 ppm and 174 ppm are due to acetate groups, which are known to be present in hemicellulose.²⁹ Some of the intensity of the 174 ppm peak could be due to other carbonyl species present in hemicellulose (e.g., CO₂H groups of uronic acids).

Spectra of the three kraft pulps are shown in Figure 6, together with the spectrum of extractives-free wood (Figure 6a) for comparison. The spectrum of the short-cook pulp (kraft 1, Figure 6b) shows substantial, but incomplete, loss of lignin relative to the lignin content of extractives-free wood. The signals assigned to the carbonyl and methyl carbons of acetate groups in hemicellulose appear to be completely absent in the spectrum of kraft 1, even when the time-domain signal is processed with a moderate exponential weighting function for sensitivity enhancement prior to Fourier transformation. However, the acetate carbon signals are not good indicators of hemicellulose content, since acetate groups can be lost selectively by hydrolysis. The high-shielding shoulder on the cellulose C-1 peak, assigned to hemicellulose, is reduced in the kraft 1 spectrum relative to its intensity in the spectrum of extractives-free wood. Further evidence of the selective depletion of hemicellulose by kraft pulping is provided by the enhanced splitting in Figure 6b of the two peaks in the 80 to 70 ppm region. Hemicellulose is known to contribute intensity in the region between these peaks.⁹ The shoulders on the cellulose C-4 and C-6 signals are reduced (but not eliminated) in the spectrum of kraft cook 1, relative to their intensities in the extractives-free wood spectrum. These observations are consistent with substantial removal of lignin and preferential loss of hemicellulose at short cook times. Preferential, but incomplete, removal of hemicellulose is known to occur in the early stages of pulping.³⁰

The spectrum of the kraft pulp obtained from an intermediate cook time (kraft 2) is shown in Figure 6c. It is readily apparent from the aromatic and methoxy regions of the spectrum that a significant further reduction in lignin content is achieved by pulping for a longer period of time. There are no apparent changes in the carbohydrate signals relative to those in Figure 6b, indicating that there are no obvious modifications in the structure or morphology of cellulose in the later stages of kraft pulping. The shoulders on the cellulose C-4 and C-6 signals in the

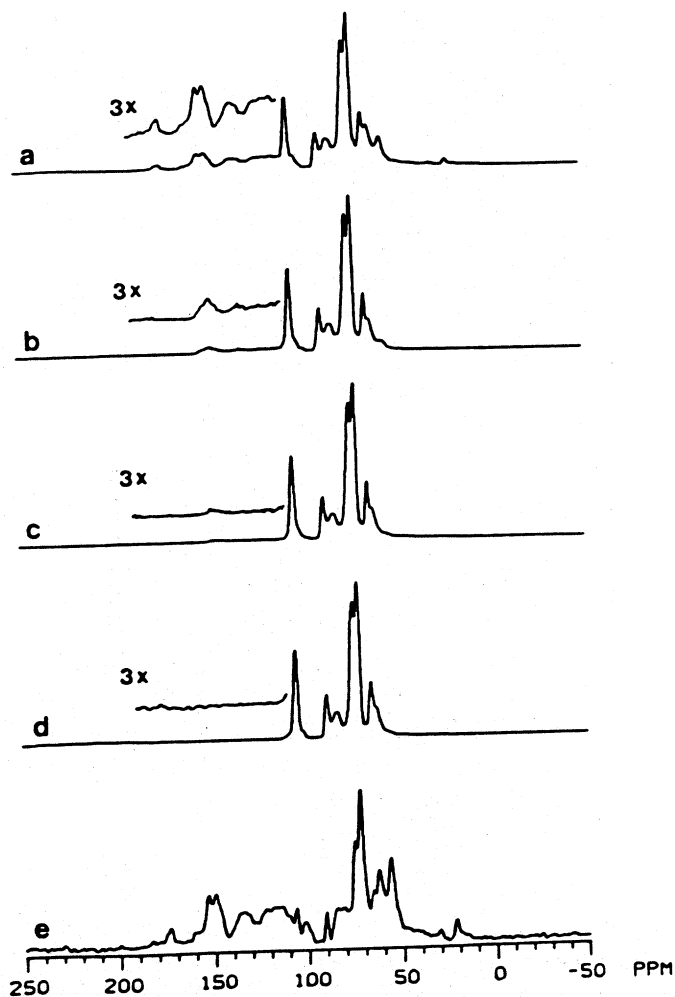


FIGURE 6. ^{13}C -CP/MAS NMR spectra of kraft pulps: (a) extractives-free wood, (b) kraft cook 1 (short cook time), (c) kraft cook 2 (intermediate cook time), (d) kraft cook 3 (long cook time), and (e) difference spectrum obtained by the subtraction of (d) from (a).

spectrum of kraft 2 pulp are identical in intensity and appearance with those in the spectrum of kraft 1 pulp. ^{13}C -CP/MAS NMR spectra of hemicellulose preparations have intensity in the regions of the C-4 and C-6 shoulders.⁹ The failure to observe further decreases in shoulder intensity with longer cook times supports the idea that selective removal of hemicellulose occurs at short cook times but not at moderate cook times.³⁰ The residual shoulders are due, in part, to cellulose.

The NMR spectrum of a kraft pulp (kraft 3) that was cooked somewhat longer than the one discussed above is shown in Figure 6d. This spectrum bears a strong resemblance to that of cellulose I.²⁰ There is no evidence in the spectrum of this pulp (or of any other pulp which were examined) for the presence of cellulose polymorphs other than cellulose I. No changes in the spectrum of this pulp were observed following overnight drying *in vacuo* at 145°C (spectrum not shown). Lignin signals are not clearly visible in Figure 6d; the lignin content by Kappa number is 2.2% for this sample. In order to show more clearly the changes in wood during kraft pulping, the spectrum of kraft pulp 3 (Figure 6d) was digitally subtracted from the spectrum of extractives-free wood (Figure 6a). Such subtractions produce difference spectra which empha-

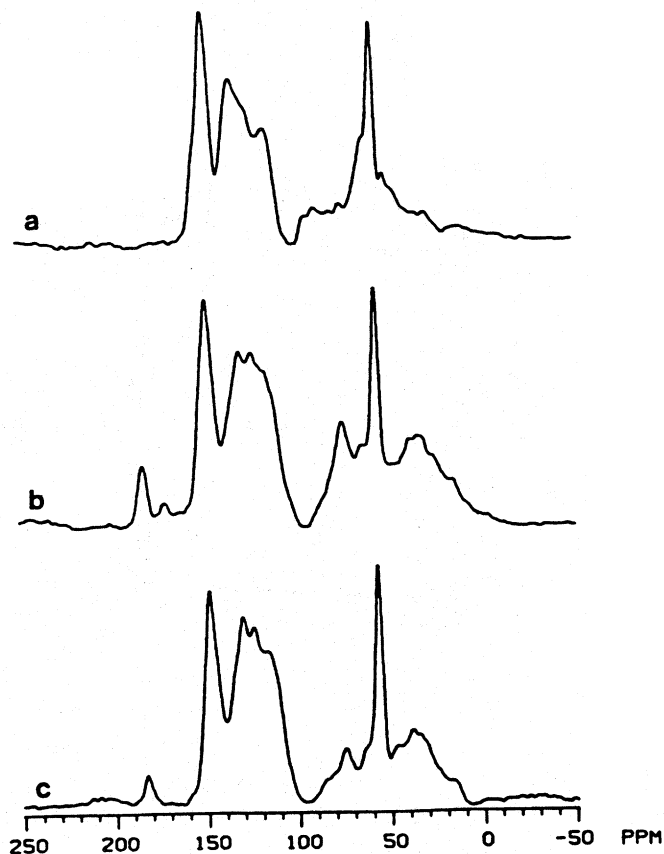


FIGURE 7. ^{13}C -CP/MAS NMR spectra of kraft lignins: (a) Klason lignin, (b) kraft cook 2 lignin, and (c) kraft cook 3 lignin.

size the features of one spectrum that are distinct from those of another spectrum. The weighting factor used in the subtraction was selected to minimize the resulting cellulose signals, without introducing negative peaks. The result of this subtraction is shown in Figure 6e. Signals from the lignin and hemicellulose components are clearly seen in this mode of presentation.

Kraft lignin preparations were obtained from kraft cooks 2 and 3 by neutralizing mother liquor samples with CO_2 ; precipitated lignin was collected by filtration. Many of the features of the kraft 2 and kraft 3 lignin spectra (Figure 7b and Figure 7c, respectively) are very similar to those in the spectrum of Klason lignin (Figure 7a). Comparisons of kraft lignins and Klason lignin must be done with caution; these two types of lignins are prepared under greatly differing conditions, and both have properties differing from those of native lignin. The spectra of the kraft lignins (Figures 7b,c) each have a signal at 183 ppm which is not present in the Klason lignin spectrum (Figure 7a) and which is consistent with carboxylate anions. This peak lies outside the range of chemical shifts of esters. Uronic acids of hemicellulose could contribute some intensity to this signal.

The spectra of the kraft lignins each have a signal at 74 ppm which is absent in the spectrum of Klason lignin. This signal is probably due to carbohydrate and resembles that of hemicellulose.⁹ The signal at 74 ppm is much smaller in Figure 7c than in Figure 7b. This presumably reflects a greater extent of alkaline hydrolysis at longer reaction times. The spectra of the kraft lignins each have a broad peak, or complex of peaks, centered at 30 to 40 ppm. This feature is of much lower intensity in the spectrum of Klason lignin.

III. CONCLUSIONS

The above three studies have illustrated the use of ^{13}C -CP/MAS NMR in the study of processes for the treatment of wood or lignin. The utility of solid state NMR for probing the chemical changes induced by such processes has been demonstrated for the specific examples of steam hydrolysis, pyrolysis, and pulping.

The most serious limitation apparent from the above studies is spectral resolution. Lignin and polysaccharides are complex polymeric materials, and highly detailed studies of structure and reactivity in the solid state will require more resolution than is currently available with existing CP/MAS techniques. Future applications of solid-state NMR to plant materials would be greatly facilitated by the development of new methods and/or the improvement of existing techniques.

The present state of the art, however, is not too bad. Substantially better resolution is observed in CP/MAS spectra of lignin than with, for example, coal. Even without further refinements in NMR methods, there is much that can still be learned from solid-state NMR studies of the chemistry of wood and lignin. Such studies will, no doubt, be forthcoming.

REFERENCES

1. Sarkanen, K. V. and Ludwig, C. H., Lignins: occurrence, formation, structure and reactions, Wiley-Interscience, New York, 1971, 695.
2. Nimz, H. H. and Ludemann, H.-D., Kohlenstoff-13-NMR-Spektren von Ligninen. VI. Lignin- und DHP-Acetate, *Holzforchung*, 30, 33, 1976.
3. Ludemann, H.-D. and Nimz, H., Carbon-13 nuclear magnetic resonance spectra of lignins, *Biochem. Biophys. Res. Commun.*, 52, 1162, 1973.
4. Nimz, H. H., Robert, D., Faix, O., and Nemr, M., Carbon-13 NMR spectra of lignins, 8. *Holzforchung*, 35, 16, 1981.
5. Yannoni, C. S., High resolution NMR in solids: the CPMAS experiment, *Acc. Chem. Res.*, 15, 201, 1982.
6. Fyfe, C. A., *Solid State NMR for Chemists*, CFC Press, Guelph, Ontario, 1983.
7. Maciel, G. E., High-resolution nuclear magnetic resonance of solids, *Science*, 226, 282, 1984.
8. Opella, S. J. and Frey, M. H., Selection of nonprotonated carbon resonance in solid-state nuclear magnetic resonance, *J. Am. Chem. Soc.*, 101, 5854, 1979.
9. Kolodziejcki, W., Frye, J. S., and Maciel, G. E., Carbon-13 nuclear magnetic resonance spectrometry with cross polarization and magic-angle spinning for analysis of lodgepole pine wood, *Anal. Chem.*, 54, 1419, 1982.
10. Taylor, M. G., Deslandes, Y., Bluhm, T., Marchessault, R. H., Vincendon, M., and Saint-Germain, J., Solid-state ^{13}C NMR characterization of wood, *Tappi*, 66(6), 92, 1983.
11. Haw, J. F., Maciel, G. E., and Schroeder, H. A., Carbon-13 nuclear magnetic resonance spectrometric study of wood and wood pulping with cross polarization and magic-angle spinning, *Anal. Chem.*, 56, 1323, 1984.
12. Haw, J. F., Maciel, G. E., and Biermann, C. J., Carbon-13 nuclear magnetic resonance study of rapid steam hydrolysis of red oak, *Holzforchung*, 38, 327, 1984.
13. Maciel, G. E., Haw, J. F., Smith, D. H., Gabrielson, B. C., and Hatfield, G. R., Carbon-13 nuclear magnetic resonance of herbaceous plants and their components using cross polarization and magic angle spinning, *J. Agric. Food Chem.*, 33, 185, 1985.
14. Haw, J. F. and Maciel, G. E., Carbon-13 nuclear magnetic resonance spectrometry of oil seeds with cross polarization and magic-angle spinning, *Anal. Chem.*, 55, 1262, 1983.
15. O'Donnell, D. J., Ackerman, J. J. H., and Maciel, G. E., Comparative study of whole seed protein and starch content via cross polarization-magic angle spinning carbon-13 nuclear magnetic resonance spectroscopy, *J. Agric. Food Chem.*, 29, 514, 1981.
16. Haw, J. F. and Schultz, T. P., Carbon-13 CP/MAS NMR and FT-IR study of low-temperature lignin pyrolysis, *Holzforchung*, 39, 289, 1985.

Nuclear Magnetic Resonance in Agriculture

17. Pfeffer, P. E., Gerasimowicz, W. V., and Piotrowski, E. G., Effect of paramagnetic iron on quantitation in carbon-13 cross polarization magic angle spinning nuclear magnetic resonance spectrometry of heterogeneous environmental matrices. *Anal. Chem.*, 56, 734, 1984.
18. Maciel, G. E., Bartuska, V. J., Ackerman, J. J. H., O'Donnell, D. J., and Hawkins, B. L., A ¹³C NMR study of four lignins in the solid and solution states. *Makromol. Chem.*, 182, 2297, 1981.
19. Bartuska, V. J., Maciel, G. E., Bolker, H. I., and Fleming, B. I., Structural studies of lignin isolation procedures ¹³C NMR. *Holzforschung*, 34, 214, 1980.
20. Atalla, R. H., Gast, J. C., Sindorf, D. W., Bartuska, V. J., and Maciel, G. E., ¹³C NMR Spectra of cellulose polymorphs. *J. Am. Chem. Soc.*, 102, 3249, 1980.
21. Earl, W. L. and VanderHart, D. L., High-resolution magic angle sample spinning ¹³C NMR of solid cellulose I. *J. Am. Chem. Soc.*, 102, 3251, 1980.
22. Earl, W. L. and VanderHart, D. L., Observations by high-resolution carbon-13 nuclear magnetic resonance of cellulose related to morphology and crystal structure. *Macromolecules*, 14, 570, 1981.
23. Haw, J. F., Maciel, G. E., Kinden, J. C., and Murphy, V. G., Carbon-13 nuclear magnetic resonance spectrometric study of autohydrolyzed and organosolv-treated lodgepole pinewood using cross polarization and magic-angle spinning. *Holzforschung*, 39, 99, 1985.
24. Biermann, C. J., Schultz, T. P., and McGinnis, G. D., Rapid steam hydrolysis/extraction of mixed hardwoods as a biomass pretreatment. *J. Wood Chem. Technol.*, 4, 111, 1984.
25. Papadopoulos, J., Chem, C.-L., and Goldstein, I. S., The behavior of lignin during hydrolysis of sweetgum wood with concentrated hydrochloric acid at moderate temperatures. *Holzforschung*, 35, 283, 1981.
26. Brezny, R., Mihalow, V., and Kovacik, V., Low temperature thermolysis of lignins I. Reaction of β-0-4 model compounds. *Holzforschung*, 37, 199, 1983.
27. Brezny, R., Surina, I., and Kosik, M., Low temperature thermolysis of lignins II. Thermofractography and thermal analysis of β-0-4 model compounds. *Holzforschung*, 38, 19, 1984.
28. Fenner, R. A. and Lephart, J. O., Examination of the thermal decomposition of kraft pine lignin by fourier transform evolved gas analysis. *J. Agric. Food Chem.*, 29, 846, 1981.
29. Browning, B. L., *The Chemistry of Wood*. R. E. Brieger, Huntington, NY, 1975.
30. Rydholm, S. A., *Pulping Processes*. Interscience, New York, 1965.

Chapter 13

PROBING METABOLISM WITH DOUBLE-CROSS POLARIZATION
SOLID-STATE NMR

George T. Coker, III and Jacob Schaefer

TABLE OF CONTENTS

I.	Introduction	372
II.	Plant Metabolism	372
A.	Amino Acid Metabolism in Developing Legumes	372
1.	Asparagine	374
2.	Allantoin	375
3.	Methionine	375
4.	Proline	375
B.	Protein Turnover	375
III.	Bacterial Metabolism	376
A.	Glyphosate	376
B.	Nitrogen Fixation	377
IV.	Insoluble Biological Matrices	379
A.	Insect Cuticle	379
B.	Bacterial Cell Wall	379
C.	Future Directions	379
V.	Technical Details	379
A.	Experimental Procedures	383
B.	Equipment	384
C.	Cost	384
VI.	Future Developments	385
A.	Detection of ^{13}C - ^{13}C Labeled Chemical Bonds by Solids NMR	385
B.	Detection of Labeled Chemical Bonds Involving One Quadrupolar Nucleus (^{13}C - ^{17}O , ^{13}C - ^2D)	385
	References	386

I. INTRODUCTION

In many studies of metabolism, investigators are interested in determining how a particular compound is either synthesized or metabolized. What they are really asking is how are chemical bonds being synthesized or broken. The typical way that this is studied is to introduce a molecule within which there is an atom which is either radioactive or an unusual stable isotope.^{1,3} The fate of the molecule is then deduced by monitoring the tagged atom. For the last several years, there has been an alternate and more direct way to monitor the fate of ¹³C-¹⁵N bonds. This procedure, double cross-polarization magic angle spinning (DCPMAS) NMR, allows the investigator to determine the percentage of ¹⁵Ns (or ¹³C) bound to ¹³C (or ¹⁵N).

NMR has several advantages over the use of radiochemistry to monitor tagged molecules. NMR allows the investigator to determine easily the chemical nature of the ¹⁵N or ¹³C. When radioisotopes are used, samples must be treated with either specific enzymes or chemicals to detect specifically labeled atoms.^{4,5} This frequently entails extensive handling of the sample with associated losses. NMR uses stable isotopes as tracers. Compounds labeled with ¹⁵N are commercially available whereas compounds labeled with ¹³N, the radioisotope of nitrogen, must be synthesized and used within 2 h³ because of the short half-life of ¹³N (10 min). Stable isotopes are nontoxic whereas radioisotopes may have deleterious effects on tissues.⁶ NMR is a nondestructive technique, thus permitting the exact same sample to be analyzed in a number of ways. NMR may obtain the same information as more conventional techniques, but at a reduced cost in time and effort (e.g., Table 1).

DCPMAS NMR is a solid-state NMR technique. There are several other advantages to using solid-state NMR vs. solution NMR. Solution NMR can only measure compounds that are rotating rapidly in solution. Solid NMR can examine cellular constituents *in vivo* that are not freely soluble, such as nucleic acids, proteins, or insoluble material, such as cell walls. In dried samples the low molecular weight compounds that are visible to solution NMR are also detected by solid NMR. The combination of high-power resonant decoupling and high-speed mechanical sample spinning has allowed liquid-like spectra to be obtained from solid material. The spectra thus obtained from solid NMR can be used to determine quantitatively the amount of a particular isotope that is present in a particular compound whereas the same is not always true of solution NMR. In succeeding sections, examples are presented in which DCPMAS NMR has been used to examine different areas of metabolism of agricultural importance.

II. PLANT METABOLISM

A. Amino Acid Metabolism in Developing Legumes

1. Asparagine

In developing cotyledons of legumes, the proper ratios of amino acids necessary for the synthesis of storage protein must be synthesized from a carbon input of sucrose and a nitrogen input of asparagine and glutamine.⁷ The mechanism by which this is regulated is not known. For example, the asparaginyl residues of protein may either be derived directly from asparagine or they may arise from *de novo* synthesis. Schaefer et al.⁸ used DCPMAS NMR to determine the extent to which these two pathways form the asparaginyl residues of seed storage protein.

Immature soybean cotyledons were grown in culture with [4-¹³C; amide-¹⁵N]asparagine, a mixture of [4-¹³C]asparagine plus [amide-¹⁵N]asparagine, or a mixture of [4-¹³C; amide-¹⁵N]asparagine plus natural abundance asparagine. After 14 d, the cotyledons were harvested, lyophilized, and extracted with 80% ethanol to remove soluble amino acids. The cotyledons were then analyzed by DCPMAS NMR (Figure 1). Two spectra from each sample were obtained. The ¹⁵N CPMAS spectra (Figure 1, top) account for all the ¹⁵N present in the sample. Double-cross difference spectra (bottom) were obtained by subtracting a ¹⁵N CPMAS spectrum from a spectrum that arises from those ¹⁵N that were not bound to ¹³C. The difference spectra represent those ¹⁵N that are bonded to ¹³C (see Section V.A for further details).

Table 1
COMPARISON OF METHODS TO
DETERMINE THE EXTENT TO
WHICH BACTERIAL
PEPTIDOGLYCAN IS
CROSS-LINKED

Conventional^a

Grow cells
 Harvest cells
 Isolate cell walls
 Digest cell walls with two enzymes that are not
 commercially available
 Gel filtration
 Assay column fractions
 Gel filtration of pooled fractions
 Assay column fractions
 Preparative electrophoresis
 Acid hydrolysis
 Amino acid analysis
 Total time ~7 d

NMR^a

Grow cells with [ϵ -¹⁵N]lysine
 Harvest cells
 Lyophilize cells
 Analyze dried cells with NMR (machine time ~1 d)
 Total time 2 d

The conventional procedure was summarized from Nakel et al.⁹ and the NMR procedure was summarized from Jacob et al.²⁴ We estimated the time necessary to do both procedures.

The ¹³C-¹⁵N amide bond of the asparaginy] residues of cotyledons fed double-labeled asparagine may arise via the direct incorporation of asparagine into protein. Alternatively, asparagine entering the cotyledons may be hydrolyzed to produce [¹⁵N]ammonium and [4-¹³C]aspartate.⁹ A ¹³C-¹⁵N bond may be introduced into protein indirectly by the resynthesis of double-labeled asparagine which is subsequently used for protein synthesis. The latter pathway was shown to exist by the formation of a ¹³C-¹⁵N bond when cotyledons were fed [4-¹³C]asparagine and [amide-¹⁵N]asparagine (Table 2). The two pathways were distinguished by measuring the extent to which natural abundance perturbs the introduction of ¹³C-¹⁵N into protein. Direct incorporation of a ¹³C-¹⁵N bond from double-labeled asparagine would not be affected by the presence of natural abundance asparagine, but the indirect pathway would be affected. The flux along these two pathways was represented by r:

$$r = \frac{f(\text{undiluted}) - f(\text{diluted})}{f(\text{undiluted}) - f(\text{diluted, calculated})}$$

where f represents the relative number of ¹⁵Ns that is bonded to ¹³C under various labeling conditions: f(undiluted) is 17, f(diluted) is 12, and f(diluted,calculated) is 8.5 (17/2) (Table 2). Thus, r = 0.6 and about 40% of the asparagine residues were formed by the direct incorporation of exogenous asparagine. These results imply that there is some mechanism by which asparagine entering the cotyledons is shunted into one pathway or the other. The basic techniques and approaches used in this experiment can easily be extended to examining the incorporation of other amino acids into protein, and purines or pyrimidines into nucleic acids.

Nuclear Magnetic Resonance in Agriculture

double-label dilution

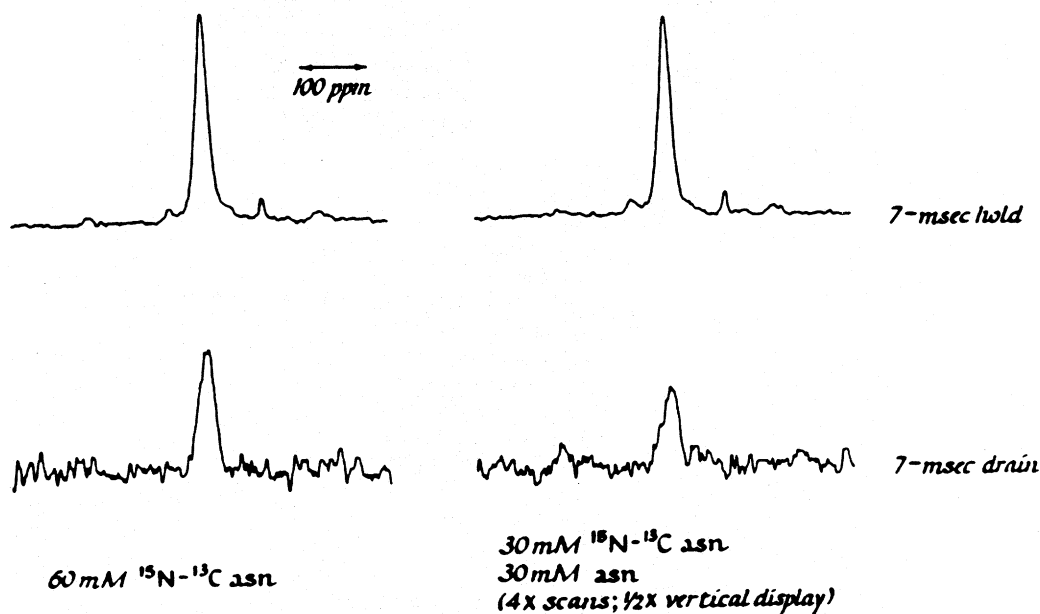


FIGURE 1. ^{15}N -CPMAS and DCPMAS NMR spectra of soybean cotyledons cultured on L-[4- ^{13}C ; ^{15}N]asparagine. Immature cotyledons were cultured for 14 d on either 60 mM double-labeled asparagine (left) or 30 mM double-labeled asparagine plus 30 mM natural abundance asparagine (right). The cotyledons were extracted with ethanol and the insoluble material was lyophilized. The top spectra represent the total ^{15}N present in the sample. The major peak represents amide nitrogen. The bottom spectra represent those ^{15}N s that are bound to ^{13}C . The bottom spectra were obtained at 6x the data accumulation as the top spectra and are displayed at 2x the vertical scale.

Table 2
INCORPORATION OF ^{15}N - ^{13}C INTO COTYLEDON
PROTEIN

Asparagine	^{15}N as % of total protein nitrogen incorporated	% amide ^{15}N adjacent to ^{13}C
30 mM [4- ^{13}C] plus 30 mM [amide- ^{15}N]	34	5
60 mM [4- ^{13}C ; amide- ^{15}N]	38	17
30 mM [4- ^{13}C ; amide- ^{15}N] plus 30 mM natural abundance	18	12

Note: Immature soybean cotyledons were grown in media containing asparagine at a final concentration of 60 mM.⁹ After 14 d, the cotyledons were harvested and lyophilized. The free amino acids were extracted with 80% ethanol. The remaining insoluble material was analyzed by ^{15}N -CPMAS NMR and ^{15}N -DCPMAS NMR.

2. Allantoin

Coker et al.¹⁰ used ^{15}N DCPMAS NMR to examine ureide metabolism in developing soybean cotyledons. The ureides, allantoin and allantoic acid, are the major forms of nitrogen transported to the shoot from the root in N_2 fixing soybeans.¹¹ To distinguish between several possible

pathways for the degradation of allantoin and the use of the nitrogen for protein synthesis. Immature cotyledons were grown in media containing allantoin labeled in specific atoms with ^{13}C and ^{15}N . By analyzing the labeled cotyledons with a combination of CPMAS and DCPMAS and DCPMAS NMR, it was determined that all of the carbon and nitrogen bonds were broken during its metabolism and the subsequent nitrogen was reassimilated via glutamine synthetase and GOGAT.

3. Methionine

The addition of methionine to cotyledons grown *in vitro* stimulated the growth of the cotyledons by 17%.¹² This was attributed to the specific enhancement of protein synthesis by additional methionine. Using ^{15}N -CPMAS NMR it was possible to quantitate how much ^{15}N in cotyledons grown with [^{15}N]methionine was present in amino acids.¹³ By examining cotyledons grown with [^{15}N]methionine with DCPMAS NMR, it was determined how much of the ^{15}N -NMR signal consisted of methionine that had not been metabolized. From these and other results, it was concluded that the high levels of exogenous methionine allow the slow step of methionine syntheses, i.e., the transfer of methyl group to homocysteine, to be bypassed and thus increase the rate at which a number of compounds can be synthesized.

4. Proline

The control of transformation of undifferentiated callus to differentiated tissue is not well understood. Certain hormone treatments and reduced sources of nitrogen are known to increase this event. Skokut et al.¹⁴ using CPMAS and DCPMAS determined the utilization of several amino acids during regeneration of alfalfa callus to embryos. Alanine and proline increased the number of embryos obtained by up to sevenfold when the proper hormones were added. When these amino acids were compared to amino acids, such as glutamate and glycine which did not enhance embryo formation, there were no differences in the uptake or utilization of nitrogen between tissues from alfalfa lines that could or could not regenerate. In tissues where regeneration was suppressed, the level of intracellular free amino acids was elevated.

When regeneration was suppressed, free proline was formed from nitrate or ammonium, and less nitrogen from proline was used in the synthesis of protein. When [^{15}N]proline was fed to the tissues, a large percentage of the proline was directly incorporated into protein as evidenced by a prominent asymmetry of the amide peak.¹⁴ The nitrogen of free proline results in a peak at 30 ppm; when present as a part of an amide bond, it results in a peak around 110 ppm. To check whether the direct incorporation of proline was a result of the synthesis of cell-wall protein which is rich in hydroxyproline, alfalfa tissue was grown with [^{13}C ; ^{15}N]proline. As measured by DCPMAS NMR, there was no difference in the metabolism of proline in regenerating and nonregenerating tissues and no evidence for enhanced cell-wall protein synthesis in nonregenerating tissues.

B. Protein Turnover

During senescence, the protein of leaves of legumes is degraded and the resulting nitrogen and carbon is shipped to the developing fruits.¹⁵ One of the questions that arises is to what extent does protein turnover prior to senescence provide nitrogen and carbon for new growth. Schaefer et al.¹⁶ used DCPMAS NMR to address this question.

Soybean plants were massively labeled with ^{15}N from $^{15}\text{NH}_4^{15}\text{NO}_3$ over a period of 7 weeks. The plants were then placed in a chamber and allowed to fix $^{13}\text{CO}_2$ for 7 d. Several leaflets of different developmental ages were harvested and lyophilized. The plants continued to grow and developmentally similar leaflets were harvested 10 to 20 d later. The exposure to $^{13}\text{CO}_2$ effectively tagged the ^{13}C - ^{15}N bonds of the protein synthesized. To the extent that this labeled protein turned over, the ^{13}C - ^{15}N bonds were broken. If a particular bond was broken, the ^{13}C will be diluted with ^{12}C or lost to the environment via photorespiration.

In a manner similar to that of the asparagine experiments (Section II.A.1 and V.A), the

Table 3
PROTEIN TURNOVER AS MEASURED BY
TURNOVER OF ^{13}C - ^{15}N BONDS

^{13}C main chain concentration		ΔT (d)	$T_{1/2}$ (d)
C1	C2		
6.9	5.6	5	20
8.5	4.2	15	17
6.1	4.3	20	45
9.1	2.2	40	20
8.2	5.9	15	38
			Avg 28

Note: Soybean plants were massively labeled with ^{15}N and then labeled with $^{13}\text{CO}_2$ for 7 d. After 1 d of labeling with $^{13}\text{CO}_2$, one trifoliate leaf was harvested. A number of days later (ΔT) a developmentally similar trifoliate was harvested. The concentration of ^{13}C in the amide bond of protein for the leaf harvested first (C1) and second (C2) was determined by ^{15}N -DCPMAS NMR as described in the text. From these values the half-life ($T_{1/2}$) of the protein was determined as described in Section II.B.

fraction of amide ^{15}N that have adjacent ^{13}C was determined. An estimate of the rate at which protein was turning over was made (Table 3). The turnover rate was determined by assuming a completely ^{15}N -labeled protein pool and a simple first-order ^{13}C scrambling of the protein, $dc/dt = -kc$ where c is the isotopic concentration of the protein carbon pool and k is the turnover rate. The time constant of the turnover was between 20 and 40 d.

III. BACTERIAL METABOLISM

A. Glyphosate

Roundup is one of the biggest selling herbicides in the world. One of the reasons for this popularity is that glyphosate, the active ingredient, is rapidly degraded in the soil. Moore et al.¹⁷ isolated a soil bacterium, PG 2982, that could grow on glyphosate as the sole source of phosphate indicating that this bacteria could break the bond between carbon and phosphorous. Jacob et al.^{18,19} using a combination of solid-state ^{13}C and ^{15}N -CPMAS and DCPMAS, deduced the pathways by which glyphosate is degraded and the regulation of these pathways in PG 2982. This is one of the few examples of NMR being used to determine metabolism which was previously unknown.

One of the initial questions was, on which side of the nitrogen is the carbon nitrogen bond broken? To answer this, cultures of PG 2982 grown on either [2- ^{13}C ; ^{15}N]glyphosate or [3- ^{13}C ; ^{15}N]glyphosate were analyzed by DCPMAS NMR. There are two major ^{15}N peaks in CPMAS NMR spectra of ethanol-extracted bacteria grown on either of the [^{15}N]glyphosates (Figure 2). The peak at 85 ppm represents nitrogen in the amide bond of protein; the peak at 215 ppm represents the N-7 found in purines. There is no double-cross difference signal in the bacteria grown on [3- ^{13}C ; ^{15}N]glyphosate demonstrating that this ^{13}C - ^{15}N bond was completely broken. In contrast, there are two prominent peaks in the difference spectrum of bacteria grown on [2- ^{13}C ; ^{15}N]glyphosate. Jacob et al.¹⁸ concluded that [2- ^{13}C ; ^{15}N]glycine formed from labeled glyphosate was used to synthesize purines and protein. They were also able to determine that the ^{13}C enrichment next to these ^{15}N was about 90% (see Section V.A). Thus glycine was incorporated intact into both purine and protein.

Jacob et al.¹⁹ extended these observations using ^{13}C -DCPMAS NMR. The same basic

PG2982 grown on labeled glyphosate

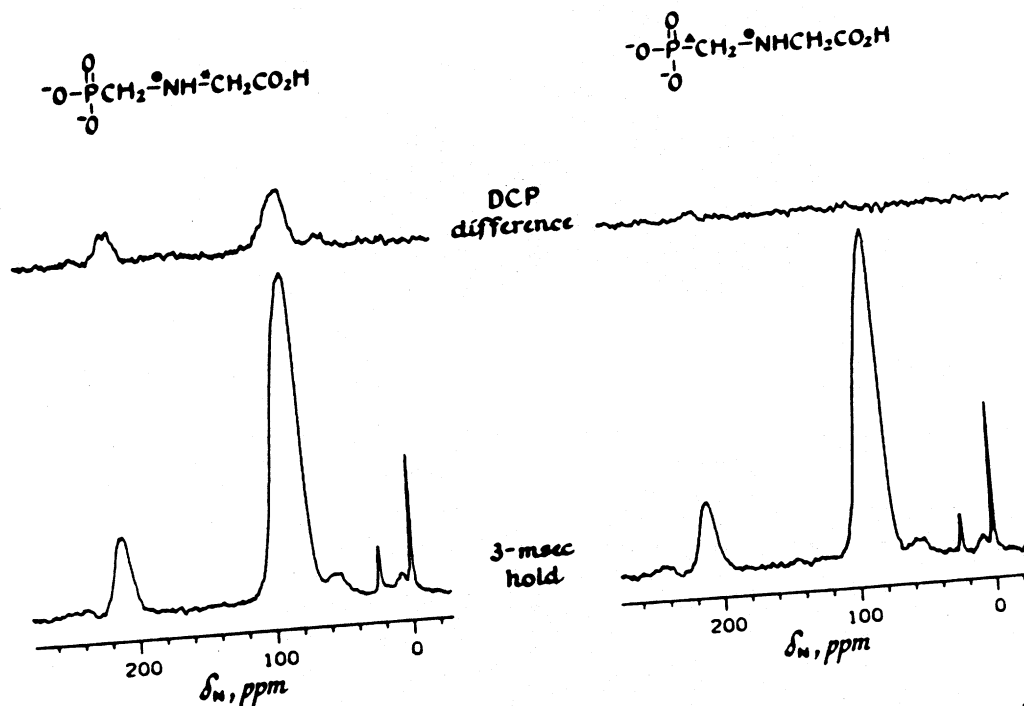


FIGURE 2. ^{15}N -DCPMAS (top) and CPMAS (bottom) NMR spectra of *Pseudomonas* PG2982 grown on [2- ^{13}C , ^{15}N]glyphosate (left) and [3- ^{13}C , ^{15}N]glyphosate (right). The peaks at 210, 85, 60, 10, and 0 ppm represent aromatic (purine), amide, guanidino, amino, and NH_4^+ nitrogen, respectively. The peak at 22 ppm is an unknown metabolite. (From Jacob, G. S., Schaefer, J., Stejskal, E. O., and McKay, R. A., *J. Biol. Chem.*, 260, 5899, 1985. With permission.)

procedures used for ^{15}N -DCPMAS NMR were employed except that the ^{13}C were polarized from the ^1H s and then the polarization of the ^{13}C was drained by adjacent ^{15}N . The ^{15}N enrichment next to ^{13}C was determined. Generally this is a more difficult experiment to analyze because of the background level ^{13}C , but this can be overcome with massive ^{13}C enrichments in the carbons of interest. Using ^{15}N -DCPMAS NMR no ^{13}C - ^{15}N bonds were found in intact cells when [3- ^{13}C ; ^{15}N]glyphosate was fed to bacteria, but with the enhanced sensitivity of ^{13}C NMR, a bond between the C-8 and N-7 of purines was found (Table 4). This bond arises from the synthesis of purines from the C-3 of glyphosate entering the tetrahydrofolate pool of C-1 intermediates and the ^{15}N of glyphosate entering via glycine. The C-2 of glyphosate also enters the same bond (Table 4). As shown by ^{13}C DCPMAS NMR, the glycine from glyphosate was incorporated intact into purines, but this depends on the cellular demand for glycine. If exogenous glycine was provided, the carbon and nitrogen were not incorporated specifically as glycine, but were integrated via general cell metabolites (Figure 3). Thus, by analyzing the end products using ^{15}N and ^{13}C solid-state NMR, Jacob et al.^{18,19} were able to map quantitatively the fluxes of glyphosate metabolism in PG 2982 without having to detect any of the intermediates.

B. Nitrogen Fixation

The synthesis of sufficient nitrogenase by *Klebsiella pneumoniae* to grow on N_2 upon exhaustion of fixed nitrogen typically takes 15 to 20 h.²⁰ This lag period can be shortened to 6 to 8 h with the addition of serine, but cannot be reduced by the addition of a number of other amino acids including glycine. Jacob et al.²¹ were able to show, using DCPMAS and CPMAS NMR, that the advantage of serine over other amino acids was that it supplied both carbon and nitrogen in the forms needed for the synthesis of ribosomal RNA which precedes the induction

Table 4
¹⁵N ENRICHMENTS OF NITROGENS OF METABOLITES
OF GLYPHOSATE IN BACTERIA

	Bond	¹⁵ N enrichment
[2- ¹³ C; ¹⁵ N]glyphosate	Amide	3
	[8-C; 7-N]purine	25
	[5-C; 7-N]purine	90
	[2-C,N]seryl residue	90
	[2-C,N]glycyl residue	90
[3- ¹³ C; ¹⁵ N]glyphosate	Amide	5
	[8-C; 7-N]purine	25

Note: Bacteria (Strain PG2982) were grown in media containing 30 mM ammonium and 1 mM of the double-labeled glyphosate as the sole sources of nitrogen. Labeled cells were harvested and lyophilized. The dried material was analyzed by DCPMAS ¹³C NMR. ¹⁵N enrichments were estimated to be ±10%.

DCPMAS ¹³C NMR of PG2982
 grown on labeled glyphosate

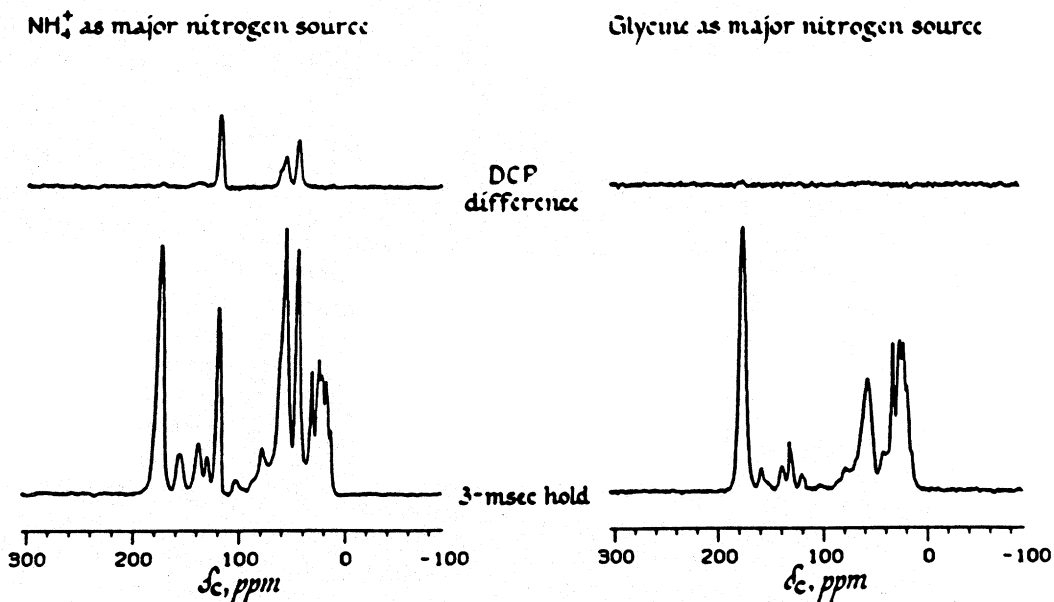
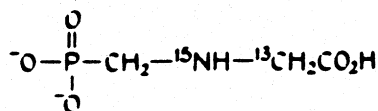


FIGURE 3. ¹³C-DCPMAS (top) and CPMAS (bottom) NMR spectra of *Pseudomonas* PG2982 grown on [2-¹³C,¹⁵N]glyphosate. The DCPMAS signals at 119, 45, and 56 ppm arise from the formation of [5-¹³C,7-¹⁵N]purine, [1-¹³C,¹⁵N]glycyl, and [2-¹³C,¹⁵N]seryl residues, respectively. (From Jacob, G. S., Garbow, J. R., Schaefer, J., and Kishore, G. M., *J. Biol. Chem.*, 262, 1522, 1987. With permission.)

nitrogenase. They were able to establish that although glycine could be used for the synthesis of the N-7 of purine, as could serine, the nitrogen of glycine was not readily used in the synthesis of the other purine nitrogens (N-1, 3, and 9).

IV. INSOLUBLE BIOLOGICAL MATRICES

Insect Cuticle

One of the major advantages to CPMAS AND DCPMAS NMR is that intact samples can be examined. Thus solid-state NMR can be used to examine materials that are not easily extracted. The structure of the cross-links in the cuticle of the tobacco hornworm was examined by Schaefer et al.²² using CPMAS and DCPMAS. Because of the difficulties in extracting material, previous workers were at best able to determine the composition of the cuticle and guess as to the nature of the bonds holding the cuticle together. Previous workers²³ proposed that the main structural components, chitin and protein, were linked directly together via cross-links formed between the epsilon groups of lysine groups and the chitin. Schaefer et al.²² examined whether lysine formed the cross-links by injecting tobacco hornworm larvae with [ϵ -¹⁵N]lysine. The depolymerized cuticles of the larvae were analyzed by ¹⁵N-CPMAS NMR. Most of the ¹⁵N labeled amino groups of lysine were scrambled to amide nitrogen and no cross-links were detected. However only 1% of the cuticular amino acids are lysine. In contrast, about 10% of the amino acids are histidine, which may also participate in cross-links. CPMAS NMR spectra of larvae fed [1,3-¹⁵N₂]histidine show that a substantial percentage of the histidyl-nitrogen was not scrambled and became part of a cross-link (Figure 4). By feeding larvae both [1,3-¹⁵N₂]histidine and dopamine labeled in the ring carbons with ¹³C, Schaefer et al.²² were able to show the formation of a ¹⁵N-¹³C bond using DCPMAS NMR (Figure 5). From this as well as additional information, they proposed a structure for the aromatic cross-link of the cuticle of tobacco hornworm (Figure 6).

B. Bacterial Cell Wall

The cell walls of bacteria consist of a peptidoglycan (Figure 7) which is held together by peptide bonds between short peptides of adjacent strands. Jacob et al.²⁴ used DCPMAS to analyze the cross-linked cell walls of bacteria. Bacteria grown with [ϵ -¹⁵N]lysine and D-[1-¹³C]alanine were harvested and subjected to ¹⁵N-DCPMAS NMR (Figure 8). Jacob et al.²⁴ found that the ¹³C-¹⁵N signal is enriched ~20%. Having previously shown that D-[1-¹³C]alanine is not scrambled they concluded that ~80% of the D-alanine for peptidoglycan arises from *de novo* synthesis. Using similar techniques, Schaefer et al.²⁴ were able to establish that there are no terminal D-alanine or D-ala-D-ala units in uncross-linked chains of the peptidoglycan.

C. Future Directions

In a similar manner, DCPMAS might be used to examine the structure of other biological matrices, such as the cell walls of higher plants. Plant cell walls consist of up to 20% protein, but the nature of the bonds holding the protein and carbohydrates together is only beginning to be unraveled.^{26,27} One protein, extensin, appears to be fixed in the cell wall by linkages between tyrosines.²⁸ Extensin also contains 7% lysine²⁹ which may be used in cross-linking the protein to other proteins, carbohydrates, or lignin. Other proteins in cell walls which contain a higher percentage of histidine³⁰ might be used for cross-linking in a manner similar to that of the insect cuticle.

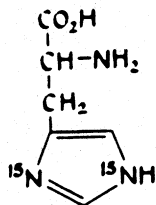
V. TECHNICAL DETAILS

A. Experimental Procedures

DCPMAS NMR is an extension of CPMAS NMR. Protons are used to polarize either carbons

Nuclear Magnetic Resonance in Agriculture

DL-[1,3-¹⁵N₂]Histidine



a. unsclerotized



b. sclerotized



c. exuviae

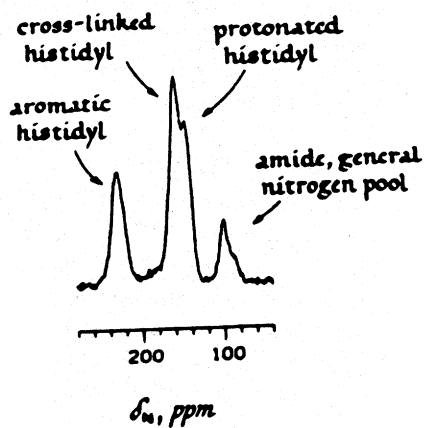


FIGURE 4. ¹⁵N-NMR of tobacco hornworm cuticle. Immature larvae were injected with L-[1,3-¹⁵N₂]histidine and sacrificed before the cuticle formed (unsclerotized), as the cuticle was forming (sclerotized), or when the cuticle was completely formed (exuviae). The material was analyzed by ¹⁵N-CPMAS NMR. The horizontal scale is in parts per million downfield from solid ammonium sulfate as an external reference. (From Schaefer, J., Kramer, K. J., Garbow, J. R., Jacob, G. S., Stejskal, E. O., Hopkins, T. L., and Speirs, R. O., *Science*, 235, 1200, 1987. With permission.)

or nitrogens (Figure 9). Then for DCPMAS NMR, the proton radio frequency is turned off and the spins of the ¹⁵N and ¹³C are allowed to interact. Because this interaction falls off as the inverse of distance to the sixth power, only ¹³C and ¹⁵N bonded together will interact. After a period of time, the spins of either ¹⁵N or ¹³C can be observed. In practice, two spectra are obtained concurrently. For example, the first pulse sequence with ¹³C radio frequency off resonance results in a CPMAS signal arising from all of the ¹⁵N present. The next pulse sequence with the

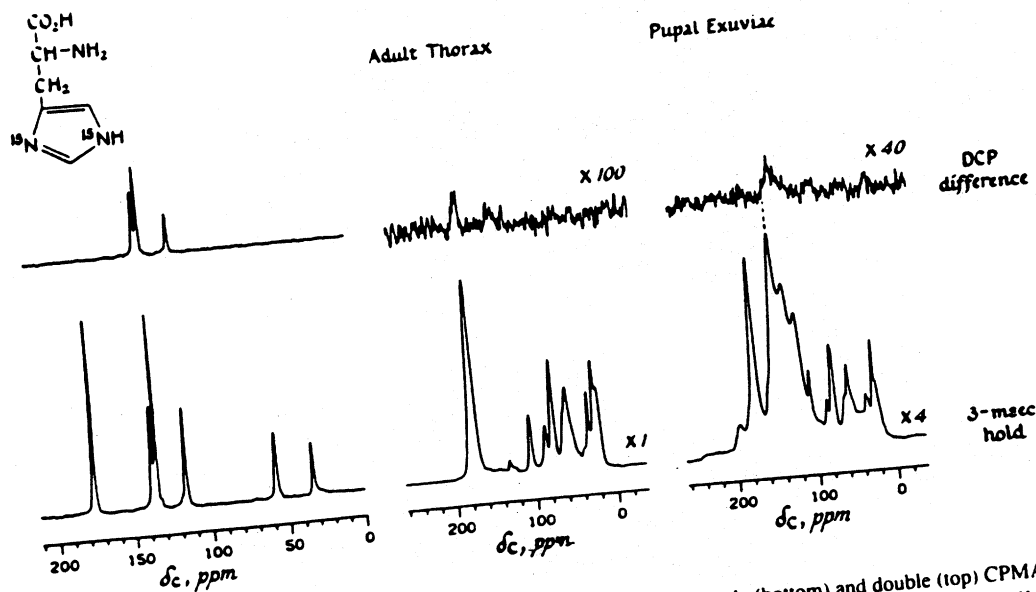


FIGURE 5. CPMAS and DCPMAS NMR of tobacco hornworm cuticle. Single (bottom) and double (top) CPMAS ^{13}C -NMR spectra of $[1,3-^{15}\text{N}]$ histidine (left), adult thoracic cuticle labeled with L- $[1,3-^{15}\text{N}]$ histidine and D- $[UL-^{13}\text{C}]$ glucose (middle), and mature pupal cuticle labeled with $[1,3-^{15}\text{N}]$ histidine and $[\text{ring-}^{13}\text{C}]$ dopamine (right) are presented. The top spectrum represents only those ^{13}C s bonded to ^{15}N (DCP difference); the bottom spectrum represents all ^{13}C s. The ^{13}C label from glucose appears predominantly in chitin peaks, such as those near 80 ppm, while that from dopamine enhances the intensity of the aromatic region of the spectrum from 120 to 160 ppm. (From Schaefer, J., Kramer, K. J., Garbow, J. R., Jacob, G. S., Stejskal, E. O., Hopkins, T. L., and Speirs, R. O., *Science*, 235, 1200, 1987. With permission.)

proposed structure

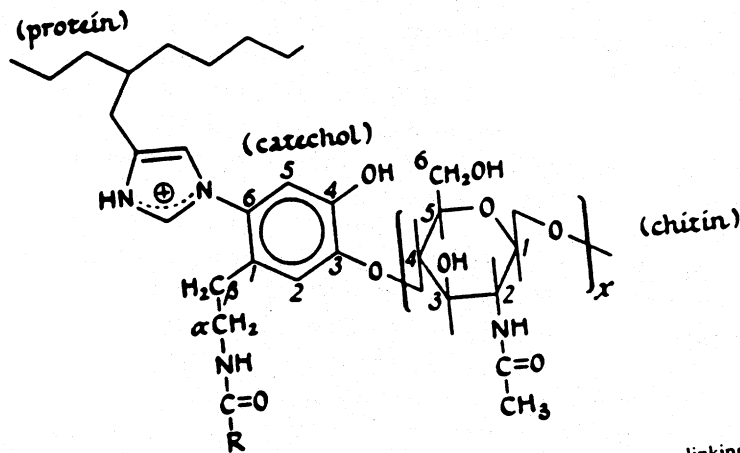


FIGURE 6. Proposed structure for tobacco hornworm cuticle cross-linking. (From Schaefer, J., Kramer, K. J., Garbow, J. R., Jacob, G. S., Stejskal, E. O., Hopkins, T. L., and Speirs, R. O., *Science*, 235, 1200, 1987. With permission.)

^{13}C radio frequency on resonance results in a DCPMAS signal representing the ^{15}N not bonded to the ^{13}C . The two spectra are subtracted from one another resulting in the DCPMAS difference spectrum. This spectrum represents the ^{15}N that is bound to ^{13}C . In a similar manner, ^{13}C DCPMAS signals can also be obtained. When the ^{13}C is on resonance, an additional drain on the ^{15}N is present such that for the ^{15}N

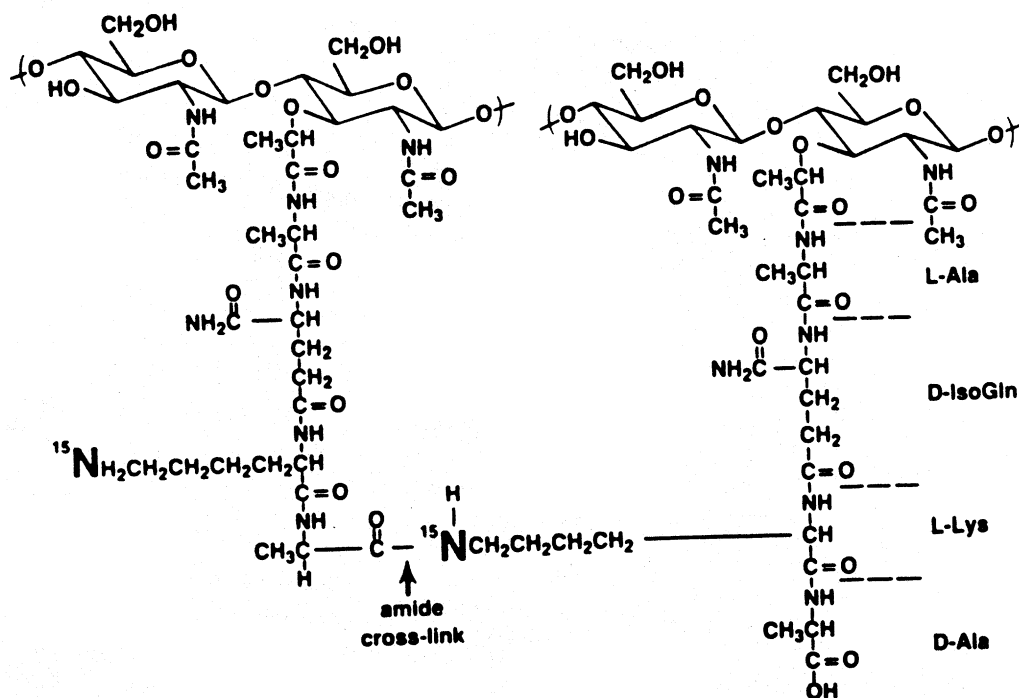


FIGURE 7. Structure of peptidoglycan.

signal $S = S_0 \exp(-t/T_d)$ where S_0 represents the signal obtained without the ^{13}C drain, t is the time that the ^{13}C and ^{15}N are allowed to interact, and T_d is the time constant for the drain. The time constant represents the efficiency by which the ^{15}N polarizes the ^{13}C . This value depends on several factors including the length of the ^{13}C - ^{15}N bond. The two spectra are subtracted from one another to obtain the relative difference spectrum, ΔS . The fraction of ^{13}C next to ^{15}N , f , can be read from Figure 10, provided the T_d for the particular bond is known. For example, in Section III, Jacob et al.¹⁸ determined the extent to which doubly labeled glycine was being incorporated intact into purines and into proteins. The ratio of the difference spectrum to that of the CPMAS spectrum for the purine signal was 0.43 and for the amide signal was 0.18. The T_d for the purine nitrogen was 5 ms and for the amide signal was 14 ms. By combining these values and reading off Figure 10, it was determined that the ^{13}C enrichment next to these ^{15}N was 90%.

The analysis is somewhat more complicated when protein turnover was being analyzed (Section II.B).¹⁶ In this case, the ^{15}N can be found in three types of linkages with respect to ^{13}C , all with different T_d s. The ^{15}N may be bound to a ^{13}C carbonyl carbon, a ^{13}C aliphatic carbon, or it may have both a ^{13}C carbonyl and a ^{13}C aliphatic carbon. Thus instead of only a single rate by which polarization is drained from ^{15}N , there are three possible rates. Schaefer et al.¹⁶ showed that these simplify to an equation with a form similar to that shown above.

B. Equipment

Only one DCPMAS spectrometer has been reported in routine use.³¹ This machine is built around an Oxford 89-mm vertical bore superconducting solenoid operating at 200 MHz for protons. The spectrometer's three radio frequency channels (^1H , ^{13}C , and ^{15}N) are each equipped with 1.5-kW transmitters. The single-coil probe is triple tuned using remote tuning elements.³²

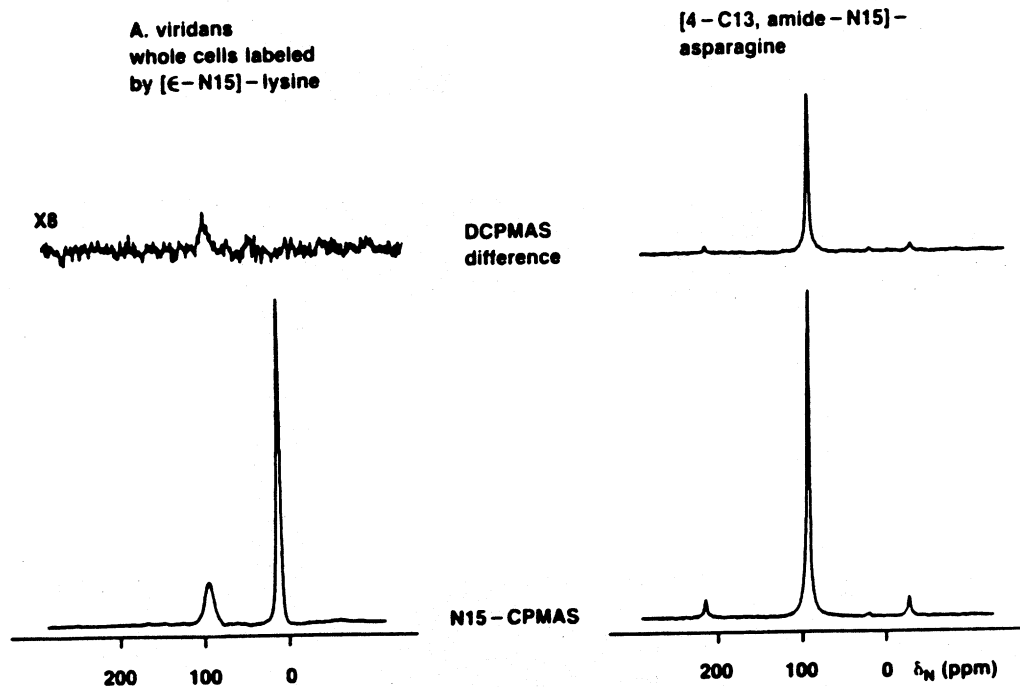


FIGURE 8. ^{15}N -CPMAS and DCPMAS NMR of lyophilized whole cells of *Aerococcus viridans* labeled with L-[ϵ - ^{15}N]lysine and DL-[1- ^{13}C]alanine. The spectrum at the top (left) represents ^{15}N bonded to ^{13}C ; the bottom (left) spectrum represents all ^{15}N . The peak at 95 ppm represents amide nitrogen and the peak at 14 ppm represents amino nitrogen. The spectra at the right was obtained from solid [4- ^{13}C ; amide- ^{15}N]asparagine.

Double-Cross Polarization Pulse Sequence

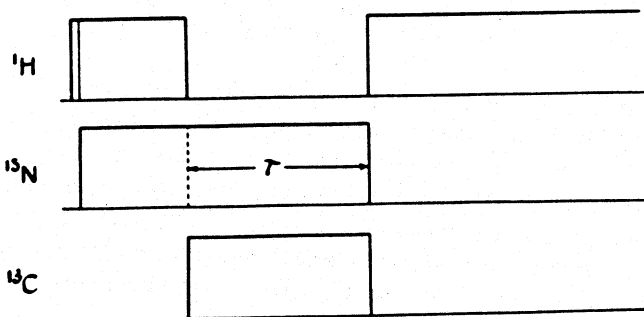


FIGURE 9. DCPMAS NMR pulse sequence. A ^{15}N direct difference signal is accumulated by shifting the ^{13}C radio frequency field off resonance for one scan and on resonance for the next. The second NMR signal is subtracted from the first. The time, t , during which the ^1H is off is called the ^{15}N hold time when the ^{13}C radio frequency field is off resonance, and the drain time when the ^{13}C is on resonance. Data acquisition occurs with the ^1H radio frequency field turned back on for dipolar decoupling.

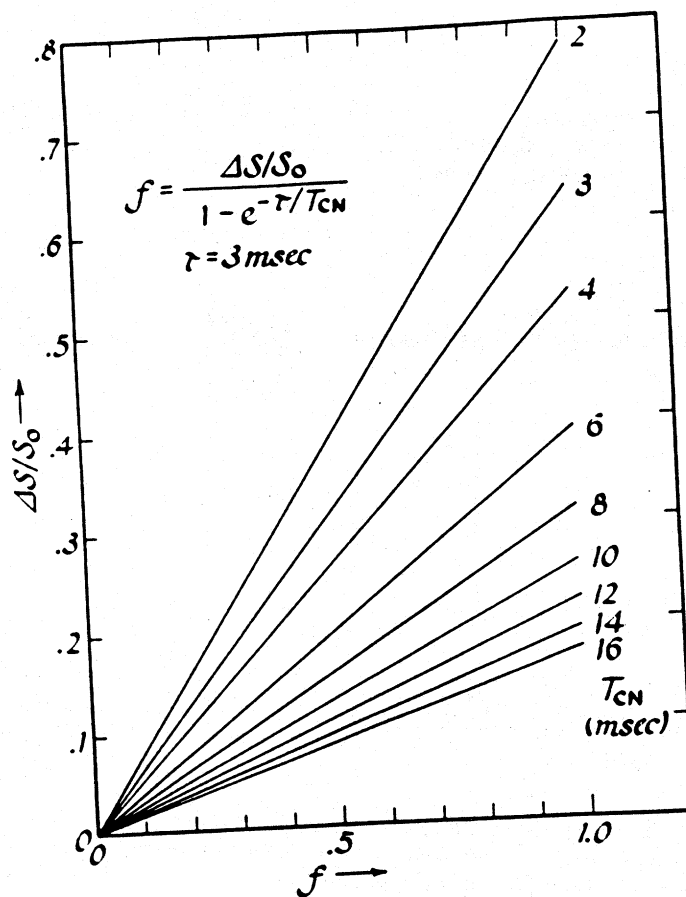


FIGURE 10. The fraction, f , of the ^{15}N atoms of a chemical bond with ^{13}C neighbors as a function of the ^{15}N DCP difference signal, ΔS , observed for a carbon-nitrogen contact time, t , of 3 ms for typical values of the carbon-nitrogen cross-polarization transfer time T_{CN} . The difference signal is scaled by the CPMAS signal after the ^{15}N spin lock, S_0 . The calculated lines correspond to $f = (\Delta S/S_0)/(1 - e^{-\tau/T_{CN}})$.

The coil is 13 mm in diameter and permits the use of rotors with a 1-g payload. In operation, both the radio frequency pulse amplitudes and the magic angle spinning speed are controlled by active feedback circuits.³³ This is necessary because of the sensitivity of the ^{13}C - ^{15}N cross-polarization transfer to slight Hartmann-Hahn mismatches. The operation of the spectrometer is monitored twice a minute by a dedicated microcomputer to ensure that no crucial parameter has drifted outside of established limits. In practice, this has meant successful 2-week long double-cross data accumulations involving 1,000,000 scans with no operator intervention.²²

C. Cost

The cost of the isotopically labeled material can vary widely. [^{13}C]sodium bicarbonate and [^{15}N]nitrate are available for as little as \$70/g. Glycine labeled either with ^{13}C or ^{15}N is \$125/g. The costs will go up dramatically for compounds that are labeled with both ^{13}C and ^{15}N in specific atoms. For example [2- ^{13}C , ^{15}N]glyphosate costs \$4000/g. However, these costs must also be balanced against the amount of time necessary to obtain similar results with other methods. A number of groups had been trying to identify the pathway of glyphosate metabolism for several years using [^{14}C]glyphosate. Jacob et al.¹⁸ using labeled glyphosate and DCPMAS NMR with one experiment were able to establish the major pathways by which glyphosate was metabo-

lized. It took about 4 man-months and 2 d of NMR time. Although radioactive isotope was cheaper per experiment, the answer was obtained more rapidly using NMR.

VI. FUTURE DEVELOPMENTS

A. Detection of ^{13}C - ^{13}C Labeled Chemical Bonds by Solids NMR

One approach to the detection of a ^{13}C - ^{13}C labeled spin pair in a biological solid is by the solid-state analog of a liquid-state 2D COSY experiment.³⁴ In this experiment, homonuclear chemical shifts are connected by the effect of scalar coupling between the labeled pair during the two-dimensional (2D) mixing time.³⁵ The coupling generates so-called "off-diagonal" peaks in a 2D contour plot. For solids, direct ^{13}C - ^{13}C dipolar coupling is weak enough that searching for minor peaks from a label, just off a dense and cluttered natural-abundance diagonal, is impractical.³⁴

Multiple-quantum coherence has also been used in liquid-state experiments to identify homonuclear labeled pairs.³⁶ Unfortunately, the solid-state version of this experiment requires choosing a pulse spacing *comparable* to the inverse of the ^{13}C - ^{13}C dipolar coupling of 2 to 4 kHz, but *short* compared to the inverse of the magic-angle spinning speed of 3 to 6 kHz. These are mutually exclusive demands. More involved multiple-quantum experiments using synchronized pulsing and spinning³⁷ overcomes this limitation, at least in part, but overall sensitivity of the multiple-quantum experiment for spinning solids is still questionable.

A more straightforward approach uses ^{13}C - ^{13}C spin diffusion to establish connectivity and so to characterize ^{13}C -labeled chemical bonds. This experiment begins with a cross-polarization transfer from protons to carbons. The resulting ^{13}C magnetization is then restored to the static magnetic field direction by a 90° pulse. The third step is selective inversion by one of the lines arising from the label by a string of weak pulses, the so-called "DANTE" irradiation.³⁸ If this magnetization is sampled immediately, inverted, and the spectrum without DANTE irradiation subtracted, the resulting difference spectrum consists only of the inverted line from the labeled carbon, together with its spinning sidebands.³⁹ The complicated natural-abundance signal has been removed. If we allow, say, 10 ms to elapse after the DANTE irradiation and before the sampling, ^{13}C - ^{13}C spin diffusion will connect carbons which are directly coupled (i.e., ^{13}C which are part of a labeled chemical bond). Spin diffusion is slow enough that more distant ^{13}C s are not connected. Now the difference spectrum will contain both the original labeled peak, and a new peak due to spin diffusion. Characteristic isotropic shifts as well as chemical shift tensors (from spinning sidebands) can be used to identify the ^{13}C -labeled bond. This method has been used successfully to identify the binding sites of [15,16- $^{13}\text{C}_2$] labeled acetylenic steroid to estradiol dehydrogenase.⁴⁰

B. Detection of Labeled Chemical Bonds Involving One Quadrupolar Nucleus (^{13}C - ^{17}O , ^{13}C - ^{2}D)

Oldfield⁴¹ has shown that CPMAS ^{17}O -NMR is possible in some inorganic solids using only the central ^{17}O transition of this spin 5/2 quadrupolar nucleus. While even the central transition may be too broad (300 kHz) to observe in biological solids (excluding phosphates) because of unfavourable ^{17}O relaxation parameters, indirect detection of ^{13}C -NMR in a double-cross polarization experiment may be practical.

The key to practicality is sensitivity. Compared to ^{13}C - ^{15}N double-cross, the ^{13}C - ^{17}O experiment is at a disadvantage because the central transition represents only about 15% of the total intensity and because commercial isotopic enrichment of ^{17}O is less than 60%. However, the ^{13}C - ^{17}O experiment is at an advantage because the ^{13}C - ^{17}O dipolar coupling is three times greater than ^{13}C - ^{15}N coupling and magic-angle spinning modulation of the transfer process may not be an interfering factor.⁴²

Possibly a simple approach to the detection of ^{13}C - ^{17}O labeled bonds is to avoid a genuine cross-polarization step altogether. Instead, by inserting ^{17}O 180° pulses synchronized with the

magic-angle rotor (one pulse every half rotor period), ^{17}O dipolar dephasing of the carbon magnetization will not refocus with each rotor period. The dephasing due to ^{13}C - ^{17}O dipolar coupling will then appear as a "drain" on the carbon magnetization. Appropriate difference spectra will reveal only those carbons coupled to ^{17}O . This is an approach similar to that suggested by Lippmaa⁴¹ for the observation of carbon chemical shift anisotropies by synchronized spinning and carbon 180° pulses.

Both this approach and the standard double cross-polarization experiment should be appropriate for the observation of ^{13}C -2D and ^{15}N -2D labeled bonds. The 2D NMR spectrum is well characterized and about 150 kHz in width.⁴⁴ Nevertheless, the motivation for developing a ^{13}C -2D double cross-polarization has been less compelling than that for ^{13}C - ^{17}O , possibly because of the popularity of 2D NMR direct detection of labels.

REFERENCES

1. Mudd, S. H. and Datko, A. H., Methionine methyl group metabolism in *Lemna*. *Plant Physiol.*, 81, 103, 1986.
2. Dungey, N. O. and Davies, D. D., Protein turnover in the attached leaves of non-stressed and stressed barley seedlings. *Planta*, 154, 435, 1982.
3. Schubert, K. R. and Coker, G. T., III, Nitrogen and carbon assimilation in N_2 -fixing plants. Short-term studies using ^{15}N and ^{13}C . in *Short-Lived Radionuclides in Chemistry and Biology*, Root, J. W. and Krohn, K. A., Eds., American Chemical Society, Washington, D.C., 1981.
4. McClure, P. R., Coker, G. T., III, and Schubert, K. R., Carbon dioxide fixation in roots and nodules of *Alnus glutinosa*. I. Role of phosphoenolpyruvate carboxylase and carbamyl phosphate synthetase in dark CO_2 fixation, citrulline synthesis, and N_2 fixation. *Plant Physiol.*, 71, 652, 1983.
5. Nakel, M., Ghuysen, J.-M., and Kandler, O., Wall peptidolycan in *Aerococcus viridans* strains 201 Evans and ATCC 11563 and in *Gaffkya homari* strain ATCC 10400. *Biochemistry*, 10, 2170, 1971.
6. Cooper, P. C. and Burgess, A. W., Biosynthetic labeling with ^{32}P : radiation damage to mammalian cells. *Anal. Biochem.*, 144, 32, 1985.
7. Rainbird, R. M., Thorne, J. H., and Hardy, R. W. F., The role of amides, amino acids and ureides in the nutrition of developing soybean seeds. *Plant Physiol.*, 74, 329, 1984.
8. Schaefer, J., Skokut, T. A., Stejskal, E. O., McKay, R. A., and Varner, J. E., Asparagine amide metabolism in developing cotyledons. *Proc. Natl. Acad. Sci. U.S.A.*, 78, 5978, 1981.
9. Skokut, T. A., Varner, J. E., Schaefer, J., Stejskal, E. O., and McKay, R. A., NMR determination of asparagine and glutamine nitrogen utilization for synthesis of storage protein in developing cotyledons of soybean in culture. *Plant Physiol.*, 69, 308, 1982.
10. Coker, G. T., III and Schaefer, J., ^{15}N and ^{13}C NMR determination of allantoin metabolism in developing soybean cotyledons. *Plant Physiol.*, 77, 129, 1985.
11. McClure, P. R., Israel D. W., and Volk, R. J., Evaluation of the relative ureide content of xylem sap as an indicator of N_2 fixation in soybeans. *Plant Physiol.*, 66, 720, 1980.
12. Thompson, J. F., Madison, J. T., Waterman, M. A., and Muenster, A-M. E., Effect of methionine on growth and protein composition of cultured soybean cotyledons. *Phytochemistry*, 20, 941, 1981.
13. Coker, G. T., III, Garbow, J. R., and Schaefer, J., ^{15}N and ^{13}C NMR determination of methionine metabolism in developing soybean cotyledons. *Plant Physiol.*, 83, 698, 1987.
14. Skokut, T. A., Manchester, J., and Schaefer, J., Regeneration in alfalfa tissue culture. Stimulation of somatic embryo production by amino acids and N-15 NMR determination of nitrogen utilization. *Plant Physiol.*, 79, 579, 1985.
15. Pate, J. S., Transport and partitioning of nitrogenous solutes. *Annu. Rev. Plant Physiol.*, 31, 313, 1980.
16. Schaefer, J., Skokut, T. A., Stejskal, E. O., McKay, R. A., and Varner, J. E., Estimation of protein turnover in soybean leaves using magic angle double cross-polarization nitrogen-15 nuclear magnetic resonance. *J. Biol. Chem.*, 256, 11574, 1981.
17. Moore, J. K., Braymer, H. D., and Larson, A. D., Isolation of a *Pseudomonas* sp. which utilizes the phosphonate herbicide glyphosate. *Appl. Environ. Microbiol.*, 46, 316, 1983.
18. Jacob, G. S., Schaefer, J., Stejskal, E. O., and McKay, R. A., Solid-state NMR determination of glyphosate metabolism in a *Pseudomonas* sp.. *J. Biol. Chem.*, 260, 5899, 1985.

19. Jacob, G. S., Garbow, J. R., Schaefer, J., and Kishore, G. M., Solid-state NMR studies of regulation of *N*-(phosphonomethyl)glycine and glycine metabolism in *Pseudomonas* sp. Strain PG2982, *J. Biol. Chem.*, 262, 1552, 1987.
20. Lindsay, H. L., Physiological Studies of Nitrogen Fixation by Cells and Cell-Free Extracts of *Aerobacter aerogenes*. Ph.D. thesis, University of Wisconsin, Madison, 1963.
21. Jacob, G. S., Schaefer, J., Garbow, J. R., and Stejskal, E. O., Solid-state NMR studies of *Klebsiella pneumoniae* grown under nitrogen-fixing conditions, *J. Biol. Chem.*, 262, 254, 1987.
22. Schaefer, J., Kramer, K. J., Garbow, J. R., Jacob, G. S., Stejskal, E. O., Hopkins, T. L., and Speirs, R. D., Direct measurement of insect cuticle cross-linking by solid-state ^{13}C and ^{15}N NMR, *Science*, 235, 1200, 1987.
23. Lipke, H., Sugumaran, M., and Henzel, W., in *Advances in Insect Physiology*. Vol. 17, Berridge, M. H., Treherne, J. E., and Wigglesworth, V. B., Eds., Academic Press, New York, 1984, 1.
24. Jacob, G. S., Schaefer, J., and Wilson, G. E., Jr., Solid-state ^{13}C and ^{15}N nuclear magnetic resonance studies of alanine metabolism in *Aerococcus viridans* (*Gaffkya homari*), *J. Biol. Chem.*, 260, 2777, 1985.
25. Schaefer, J., Garbow, J. R., Jacob, G. S., Forrest, T. M., and Wilson, G. E., Jr., Characterization of peptidoglycan stem lengths by solid-state ^{13}C and ^{15}N NMR, *Biochem. Biophys. Res. Commun.*, 137, 736, 1986.
26. Lampert, D. T. A. and Epstein, L., in *Current Topics in Plant Biochemistry and Physiology*. Vol. 2, Randall, D. D., Blevins, D. G., Larson, R. L., and Rapp, B. J., Eds., University of Missouri, Columbia, 1983, 73.
27. Cooper, J. B., Chen, J. A., and Varner, J. E., in *Structure, Function, and Biosynthesis of Plant Cell Walls*. Dugger, W. M. and Bartnicki-Garcia, S., Eds., American Society of Plant Physiologists, Rockville, MD, 1984, 75.
28. Fry, S. C., Isodityrosine, a new cross-linking amino acid from plant cell wall glycoprotein, *Biochem. J.*, 204, 449, 1982.
29. Van Holst, G. J. and Varner, J. E., Reinforced polyproline II conformation in a hydroxyproline rich cell wall glycoprotein from carrot root, *Plant Physiol.*, 74, 247, 1984.
30. Stevenson, T. T., McNeil, M., Darvill, A. G., and Albersheim, P., Structure of plant cell walls. XVIII. An analysis of the extracellular polysaccharides of suspension cultured sycamore cells, *Plant Physiol.*, 80, 1012, 1986.
31. Schaefer, J., McKay, R. A., and Stejskal, E. O., Double cross-polarization NMR of solids, *J. Magn. Reson.*, 34, 443, 1979.
32. McKay, R. A., U.S. Patent 4,446,431 (May 1, 1984).
33. McKay, R. A., 10th Annual Meeting of the Federation of Analytical Chemistry and Spectroscopy Societies, Philadelphia, September 1983.
34. Menger, E. M., Vega, S., and Griffin, R. G., Double-quantum observation of carbon couplings in solids, *J. Magn. Reson.*, 56, 338, 1984.
35. Freeman, R. and Morris, G. A., Experimental chemical-shift correlation maps in nuclear magnetic resonance spectroscopy, *J. Chem. Soc. Chem. Commun.*, 684, 1978.
36. Bax, A., Freeman, R., and Frenkiel, T. A., An NMR technique for tracing out the carbon skeleton of an organic molecule, *J. Am. Chem. Soc.*, 103, 2102, 1981.
37. Meier, B. H. and Earl, W. L., Excitation of multiple quantum transitions under magic angle spinning, *J. Chem. Phys.*, 85, 4905, 1986.
38. Morris, G. A. and Freeman, R., Selective excitation in Fourier-transform nuclear magnetic resonance, *J. Magn. Reson.*, 29, 433, 1978.
39. Caravatti, P., Bodenhausen, G., and Ernst, R. R., Selective pulse experiments in high-resolution solid-state NMR, *J. Magn. Reson.*, 55, 88, 1983.
40. Auchus, R. J., Covey, D. F., Bork, V., and Schaefer, J., Solid-state NMR observation of cysteine and lysine Michael adducts of inactivated estradiol dehydrogenase, *J. Biol. Chem.*, 263, 11640, 1988.
41. Oldfield, E., 13th Annual Meeting of the Federation of Analytical Chemistry and Spectroscopy Societies, St. Louis, September 28 to October 3, 1986; Waltar, T. H., Turner, G. L., and Oldfield, E., Oxygen-17. Cross-polarization NMR spectroscopy of inorganic solids, *J. Magn. Reson.*, 76, 106, 1988.
42. Schaefer, J., Stejskal, E. O., Garbow, J. R., and McKay, R. A., Quantitative determination of the concentrations of ^{13}C - ^{15}N chemical bonds by double cross-polarization NMR, *J. Magn. Reson.*, 59, 150, 1984.
43. Lippmaa, E., Alla, M., and Tuherm, T., in *Proc. XIX Cong. Ampere*, Heidelberg, West Germany, 1977, 113.
44. Spiess, H. W., Molecular dynamics of solid polymers as revealed by deuterium NMR, *Colloid Polym. Sci.*, 261, 193, 1983.